Experimental Characterization of a Solid Oxide Fuel Cell Coupled to a Steam-Driven Micro Anode Off-Gas Recirculation Fan

Patrick Hubert Wagner[a], Zacharie Wuillemin[b,c], David Constantin[b], Stefan Diethelm[b,c], Jan Van herle[b], Jürg Schiffmann[a,*]

[a] *Laboratory for Applied Mechanical Design (LAMD), Institute of Mechanical Engineering (IGM), Ecole Polytechnique Fédérale de Lausanne (EPFL), Neuchâtel, 2000, Switzerland*
[b] *Group of Energy Materials (GEM), IGM, EPFL, Sion, 1951, Switzerland*
[c] *SOLIDpower SA, Yverdons-les-Bains, 1400, Switzerland*

Abstract

While the global fuel utilization of solid oxide fuel cells (SOFCs) is limited by the stack aging rate, the fuel excess is typically used in a burner, and thus limiting the system electrical efficiency. Further, natural-gas-fueled SOFCs require treated water for the steam reforming process, which increases operational cost.

Here, we introduce a novel micro anode off-gas recirculation fan that is driven by a partial-admission (21 %) and low-reaction (15 %) steam turbine with a tip diameter of 15 mm. The 30 W turbine is propelled by pressurized steam, which is generated from the excess stack heat. The shaft runs on dynamic steam-lubricated bearings and rotates up to 175 000 rpm.

For a global fuel utilization of 75 % and a constant fuel mass flow rate, the electrical gross DC efficiency based on the lower heating value was improved from 52 % to 57 % with the anode off-gas recirculation, while the local fuel

*Corresponding author. E-mail address: jurg.schiffmann@epfl.ch

utilization decreased from 75 % to 61 %, which is expected to significantly increase stack lifetime. For a global fuel utilization of 85 %, gross efficiencies of 66 % in part load (4.5 kW_e) and 61 % in full load (6.3 kW_e) were achieved with the anode off-gas recirculation. The results suggest that the steam-driven anode off-gas recirculation can achieve a neutral water consumption.
Keywords: solid oxide fuel cell, anode off-gas recirculation, small-scale turbomachinery, radial fan, steam turbine, gas bearings

---

Highlights:

- First realized SOFC system with steam-driven anode off-gas recirculation fan
- Design of a novel oil-free and durable recirculation fan with gas film bearings
- Propulsion with steam turbine leads to explosion-proof and efficient fan operation
- One of the smallest steam turbines tested with a tip diameter of 15 mm
- Reliable method of measuring recirculation ratios with a double Venturi nozzle

1. Introduction

The combination of steam-reforming solid oxide fuel cell (SOFC) systems with anode off-gas recirculation (AOR) leads to (1) higher efficiency due to higher global fuel utilization (FU), (2) higher life time due to lower local FU, and (3) water-neutral operation, i.e., without water supply and treatment. A recirculation unit is needed to overcome the pressure loss of the SOFC

stack, reformer, heat exchangers, and piping. Besides fuel- and steam-driven ejectors, recirculation fans are commonly used. Table 1 gives research (top), pre-commercial (middle), and commercial (bottom) systems with AOR. The table lists nine variables: (1) the cell potential (U_{cell}), (2) the electrical gross DC power

$$P_{gross,DC} = z_{layer} U_{cell} I \tag{1}$$

that is a function of the current (I) and the number of cell layers (z_{layer}), (3) the electrical gross DC efficiency

$$\eta_{gross,DC} = \frac{P_{gross,DC}}{\dot{n}_{fuel} LHV_{fuel}} \tag{2}$$

based on the fuel molar flow rate ($\dot{n}_{fuel}$) and the fuel lower heating value (LHV), (4) the electrical net DC efficiency

$$\eta_{net,DC} = \frac{P_{gross,DC} - P_{aux}}{\dot{n}_{fuel} LHV_{fuel}} \tag{3}$$

including the auxiliary equipment power (P_{aux}), e.g., blowers, pumps, controls, and communications, (5) the electrical net AC efficiency

$$\eta_{net,AC} = \frac{P_{gross,DC} - P_{aux}}{\dot{n}_{fuel} LHV_{fuel}} \eta_{DC/AC} \tag{4}$$

including an DC/AC converter efficiency ($\eta_{DC/AC}$), (6) the global fuel utilization, referred to as the FU in this article,

$$f_{u,global} = \frac{\dot{n}_{fuel,in} - \dot{n}_{fuel,out}}{\dot{n}_{fuel,in}} \tag{5}$$

considerin the system inlet ($\dot{n}_{fuel,in}$) and system outlet fuel molar flow rate ($\dot{n}_{fuel,out}$), (7) the anode off-gas recirculation ratio (RR)

$$RR = \frac{\dot{n}_{AOR}}{\dot{n}_{AO}} \tag{6}$$

that is the ratio of the recirculated anode off-gas molar flow rate ($\dot{n}_{AOR}$) to the total anode off-gas molar flow rate ($\dot{n}_{AO}$), (8) the cell current density

$$i = \frac{I}{A_{cell}} \tag{7}$$

considering the active cell area (A_{cell}) in cm^2, and (9) the stack power density

$$\boldsymbol{p} = \frac{P_{gross,DC}}{A_{total}} = \frac{P_{gross,DC}}{z_{cell} A_{cell}} \tag{8}$$

considering the total cell area (A_{total}) in cm^2. Within this section, the gross DC power is referred to as "power" and the electrical gross DC efficiencies based on the fuel LHV is referred to as "efficiency".

Table 1 lists non-formatted values, that are experimentally measured variables and ca be directly extracted from the given references. *Italic* values were estimated with a calculation or a simulation by the authors of the reference. The authors of this paper computed and estimated the **bold** and underlined values, respectively, with the information given in the reference.

According to the authors' knowledge, the commercial product "Energy Server 5" by Bloom Energy and "BlueGen" by SOLIDpower achieve the highest electrical net AC efficiency of up to 65 % and 60 %, respectively for an electrical net AC power of 250 kW_e and 1.5 kW_e, respectively, for an SOFC power unit and an domestic-scale cogeneration SOFC system (heat and power), respectively.

According to the authors' knowledge, the first published proof-of-concept SOFC system with an AOR fan is by Noponen et al. [1] in the year of 2010. A net AC efficiency of 47 % was reached with a multi-stack assembly and

lean landfill gas.

In 2011, both Siemens [2] and Halinen et al. [3] published experimental results of an SOFC system with an AOR fan.

Halinen et al. [3] operated a 9.8 kW_e planar cross-flow SOFC with an efficiency of 59.8 % and an electrical net AC efficiency of 43 %. In 2015, Halinen [4] could improve the electrical net AC efficiency by reducing the auxiliary power and current collection losses to 50 %. In total, they operated the system over 10 000 h. A 100 W_e "high-temperature recycle blower" was used for the AOR.

Siemens [2] operated the 9.8 kW_e planar SOFC "POCD8R0" SOFC stack based on delta cells for 5314 h. The anode off-gas was recirculated with a fuel-driven ejector. For an average stack temperature of 969 °C, the estimated efficiency is 38 % (electrical gross DC efficiency based on the higher heating value of 32.3 % is reported for a fuel mixture of hydrogen, natural gas, and nitrogen). The successor system "POCD8R1" used a 360 mm fan with a rotational speed of up to 4 krpm from the Japanese company Creative Applications for the AOR.

In 2007, Rolls-Royce Fuel Cell Systems [5] announced to operate a 250 kW_e pressurized SOFC system with planar cells. The pressurization of up to 7 bar should be achieved with an in-house designed "two shaft turbo-generator" with a high- and a low-pressure turbine and compressor stage. In 2012, the company was renamed to LG Fuel Cell Systems. LG [6] gave a detailed flowsheet of the 250 kW_e SOFC: The AOR is realized with a fuel-driven ejector. The burned cathode and anode off-gas feeds the "two shaft turbo-generator". This unit generates electricity and compresses the cathode airflow. The cath-

ode off-gas recirculation is realized with an air-driven ejector. In 2018, LG [7] tested the final system over 1800 h with a power of 262 kW_e and an efficiency of 61 % and a net AC efficiency of 55 % (FU of 79 %, average stack temperature of 864 °C).

Powell et al. [8] experimentally demonstrated a planar SOFC system with AOR. They reported a power output between 1.9 kW_e and 2.6 kW_e, reaching efficiencies of 63 % and 57 %, for a global FU of 93 % and 86 %, respectively, and for a recirculation ratio of 86 %. They used an "excess-capacity blower [authors' note: side channel blower with a magnetic coupling from Airtech West] for the testing (...) to avoid the cost of a custom blower designed for high inlet temperatures", since no "properly sized blowers" for the AOR were available. The anode blower efficiency was typically 8 %.

FuelCell Energy [9] tested a 55.8 kW_e SOFC system with AOR, reaching an efficiency of 61 % for a fuel utilization of 85 %. The stack used planar cells and operated at ambient pressure. The anode off-gas is mixed with fresh incoming methane. An "anode recycle blower" from the New York Blower Company compressed this mixture and sent it to the steam reformer and to the SOFC anode. It had a diameter of 690 mm and a rotational speed of 3.75 krpm, resulting in a pressure rise of 37 mbar, a power of 1.8 kW, and an overall blower efficiency of 12 %.

Peters et al. [10] operated a planar SOFC stack at 2.5 kW_e and 4 kW_e with AOR, reaching efficiencies of 64 % and 60.5 % for a recirculation ratio of 74 % and 73 % and an average stack temperature of 728 °C and 762 °C, respectively for a global FU of 90 %. They claim that if a new stack had been used instead of an aged one, the efficiency would have been at least five percentage

points higher. An electrically-driven "hermetic side-channel blower" with a magnetic coupling from AirTech West was used.
Bosch [11] announced a "plug and play" 10 kW_e SOFC equipped with AOR, reaching an efficiency of 70 %. No further details were published so far.

Both Powell et al. [8] and Peters et al. [10] used a rolling-element-supported AOR fan, which was coupled to the electric motor with a magnetic coupling. The literature also provides examples of directly-coupled fans supported on ball bearings, e.g., by Creative Applications [12], dynamic oil film bearings, e.g., by AVL [13], or dynamic gas film bearings. The latter option has the advantage of oil-free operation, resilience to high temperatures, and a long life time, which makes this concept particularly interesting for SOFC systems. Designs by R&D Dynamics [14] and Mohawk Technologies [15] used gas foil journal and thrust bearings. According to the authors' knowledge, no reference is available that describes the experimental results of an AOR fan supported on gas film bearings coupled to an SOFC system.
Wagner et al. [16] presented the design of a novel AOR fan supported on herringbone-grooved journal and spiral-grooved thrust gas film bearings. Due to the relatively low AOR mass flow rate and relatively high fan pressure rise for a 10 kW_e SOFC system, the fan has a tip diameter of 19.2 mm and rotates up to 175 krpm. Prior to coupling this AOR fan with an SOFC system, the fan was experimentally characterized with air at 200 °C. At nominal operation of 168 krpm, the measured inlet mass flow rate was 4.9 $kg\,h^{-1}$, reaching a total-to-total pressure rise of 55 mbar, and an isentropic total-to-total efficiency 55 %, requiring a power of 18.3 W.

The objective of this paper is thus to couple this steam-driven AOR fan supported on gas film bearings to an SOFC stack and to demonstrate the feasibility of such a system. Both SOFC stack with the AOR fan and without AOR are characterized.

2. SOFC system with steam-driven AOR fan

The previously mentioned AOR fan concept introduced by Wagner et al. [16] was coupled to a 6 kW_e SOFC system. Instead of using an electrically-driven AOR fan, the new AOR concept is propelled by a 15 mm tip diameter, partial-admission (21 %), and low-reaction (15 %) steam turbine.

Steam-driven AOR fan: Figure 1 a) shows the rotor of this steam-driven AOR fan, the fan-turbine unit (FTU). On the left side is the radial AOR fan and on the right side the radial-inflow steam turbine. The 4x4 fan rotor blades have a constant blade height of 1.90 mm and a blade tip clearance of 0.14 mm. Figure 1 b) shows the turbine stator (left) and rotor blades (right), that have a radial chord of 1 mm, a constant blade height of 0.59 mm and a blade tip clearance of 0.13 mm. The full set of geometrical parameters is listed by Wagner [17]. Both the fan and turbine impeller are directly coupled with the gas-bearing-supported rotor that is coated with diamond-like carbon (DLC). The V-shapes on the rotor indicate the positions of the herringbone- grooved journal bearings. The entire unit is manufactured with turning, milling, and surface finishing operations, i.e., grinding and honing.

SOFC system with thermally-driven AOR fan: Figure 2 gives a

schematic overview of this novel SOFC system with the thermally-driven AOR fan. Both the SOFC and the FTU are in the same hot box. At the nominal operating point, natural gas is injected (stream 1 in Figure 2). The fuel is mixed with the recirculated anode off-gas (stream 7) that contains mainly deionized and neutral water vapor, carbon dioxide, and non-reacted hydrogen. Within the steam reformer, the fuel reacts with the water vapor to hydrogen and carbon monoxide (steam reforming reaction). The carbon monoxide itself reacts with the water vapor to hydrogen and carbon dioxide (water-gas shift reaction). Part of the fuel can be reformed inside the stack (internal reforming) for maximization of the system net efficiency. Internal reforming leads to a quenching effect of both the cathode and the anode. On the cathode side, this quenching effect enables a lower cathode air mass flow rate due to lower stack cooling demands. This results in a lower cathode fan power, and thus in a higher electrical net efficiency of the system. On the anode side, this quenching effect leads to a lower cell and system efficiency. The optimal amount of external reforming is thus a trade-off between cathode fan power and cell efficiency.

The planar co-flow SOFC stack anode is fueled at 710 °C (stream 3). The air at the cathode inlet has a similar temperature of 710 °C, corresponding to the temperature of the electrical oven. The heat exchanger (HEX) for heating the air (stream 24) to 710 °C is not shown in Figure 2. The anode off-gas (stream 4) has a temperature on the order of 800 °C; it is split into one part (stream 8) that is burned and another part (stream 5) that is recirculated to the steam reformer and to the anode inlet. Wagner et al. [18] suggested that a cold AOR leads to 0.5 % points higher electrical net efficiency compared to

hot AOR, for the case of a 10 kW_e system with a conventional electrically-driven AOR fan. Since the system efficiency with cold AOR is expected to be higher and the FTU design is less complicated, a recirculation temperature of 200 °C was chosen for this proof-of-concept. However, this design needs an additional HEX at stream 4 and/or 5 to cool the anode off-gas from 800 °C to 200 °C. This leads to increased system cost and increased heat losses on the one hand, but increases the electrical net efficiency and mitigates the operational risk of the AOR fan on the other. The temperature difference between the steam turbine and the AOR fan should be low to avoid the risk of a bearing failure, since the nominal clearance between the rotating shaft and the non-rotating journal bearings is only a few micrometers; a too high differential thermal expansion between the journal bearing and the rotor could lead to a potential failure. For the first steam-driven AOR fan prototype, it was decided to maintain the mean fan temperature (stream 5 and stream 6) on the same order as the mean steam turbine temperature (stream 18 and 19), which results in a turbine inlet temperature (stream 18) of 220 °C. This limits the turbine power and efficiency, but allows for a safe operation of the FTU.

The FTU was designed in such that neither external water, nor external heat is necessary at nominal operation. Heat can be recovered internally with a HEX downstream of the burner. This HEX can provide heat to the anode preheating (stream 2), steam reformer, and evaporator. The burner inlet stream (stream 8) contains uncondensed water vapor, carbon dioxide, unreacted hydrogen, and potentially unreformed carbon monoxide and natural gas (here assumed as methane). The latter three can be burned. A fan draws

ambient air (stream 26) to the burner (stream 27) to control the flame temperature, and thus the burner outlet temperature (stream 10). The burner off-gas (stream 11) is cooled and partially condensed and exits to the chimney at a temperature of 60 °C (stream 9). Water can be recovered internally from the anode off-gas (stream 11) for a water-neutral operation, i.e., the mass flow rate in stream 14 is zero. Excess water exits the system at stream 13. The pressure of the remaining water is increased by a pump to compensate the pressure loss in the evaporator and the turbine expansion; the total pressure at the turbine inlet (stream 18) is on the order of 2 bar. The water vapor is preheated, evaporated, and superheated, so that the turbine inlet total temperature is on the order of 220 °C. Part of the expanded steam (stream 20) is fed back to the condenser and another part (stream 21) exits the system through a chimney (or can be condensed).

Comparison to electrically-driven fans: Firstly, the FTU is per se explosion-proof, since no electrical components are used. This also allows for a less complicated design at high temperatures (anode off-gas temperature on the order of 800 °C). Secondly, heat cogeneration in the SOFC system is used to propel the AOR fan. Thus, the sole auxiliary electric power for the proposed AOR concept is the pump power. Due to the higher density of ambient water (998 $\mathrm{kg\,m^{-3}}$), compared to the 200 °C anode off-gas (between 0.5 $\mathrm{kg\,m^{-3}}$ to 0.6 $\mathrm{kg\,m^{-3}}$ for the presented experiments), the auxiliary power consumption is reduced. Wagner [17] suggested an improvement of the electrical net DC efficiency by 0.5 % for a 10 $\mathrm{kW_e}$ system, compared to a similar system with electrically-driven AOR fan (efficiency of 64.9 %) [18]. The main

disadvantage of the FTU in comparison to the electrically-driven AOR fan is the reduced flexibility: The power of the turbine, and thus of the fan is limited by the internal heat recovery and the fan response is slower due to the thermal inertia of the system.

Comparison to ejectors: Fuel-driven and steam-driven ejectors are commonly used for AOR. Engelbracht et al. [19] compared both AOR systems for a 5 kW_e SOFC system. The system with steam-driven ejector has an electrical net DC efficiency of 61.4 %. Thus, it is 3.3 % more efficient compared to the fuel-driven ejector system, due to the use of a pump instead of a fuel compressor. In terms of the part-load behavior, the fuel-driven ejector is limited by carbon deposition to a minimal load of 78 % for a FU of 70 %. The steam-driven ejector is limited by the condensation temperature of the anode off-gas to a load of 38 % (FU of 70 %). The condensed water is not sufficient at such low loads to supply the steam-driven ejector.
In contrast to the ejector systems, the steam-driven fan can operate in low part-load (assuming sufficient internal heat recovery for the evaporator):

- Carbon composition: The AOR can be chosen sufficiently high to prevent carbon composition.
- Water supply: The steam from the turbine can be directly recirculated to the condenser. This is possible, since the AOR and the steam are separated, which is the main difference between the steam-driven fan and the steam-driven ejector.

The separation of the anode off-gas and the steam also enables higher system efficiencies, since the AOR is not diluted. [17] The main advantages of

the steam-driven fan is thus (1) higher flexibility and (2) higher efficiency compared to a steam-driven ejector.
The main disadvantage in comparison to the ejector systems is (1) the presence of rotating parts and (2) the low entrainment ratio (AOR mass flow rate divide by turbine steam mass flow rate). Values between 1.1 and 1.4 were measured for the presented experiments. Thus, the internal heat recovery for the evaporator can be critical, depending on the state of the SOFC system and its specific heat exchanger network design.

3. Test rig setup

In order to simplify the control and the operation of the complete coupled system, the realized proof-of-concept (Figure 3) has several differences to the previously described concept of an SOFC system with a thermally-driven AOR fan (Figure 2). This leads, among other things, to a limitation of the electrical net efficiency and the utilization ratio (cogeneration of electricity and heat). Both of these values are not measured within the conducted experimental campaigns. The simplifications with regards to concept in Figure 2 are summarized as follows:

- The majority of the reforming ($83\,\% - 96\,\%$) occurred externally in the steam reformer, that was placed inside the electrical oven. The steam reformer outlet temperature (stream 3 in Figure 3) was equal to the electrical oven temperature ($710\,^{\circ}\mathrm{C}$). In this study, the amount of external reforming was not optimized and varied with the AOR and the amount of injected water vapor, used during the system start-up.

- The steam-to-methane ratio before the reformer

$$S/CH4 = \frac{\dot{n}_{2,H_2O}}{\dot{n}_{2,CH_4}} \tag{9}$$

was between 1.0 and 2.3, whereas the oxygen-to-carbon ratio before the reformer

$$O/C = \frac{\dot{n}_{2,O}}{\dot{n}_{2,C}} = \frac{\dot{n}_{2,H2O} + \dot{n}_{2,CO} + 2\dot{n}_{2,CO2}}{\dot{n}_{2,CO} + \dot{n}_{2,CO2} + \dot{n}_{2,CH4}} \tag{10}$$

was between 1.3 and 2.2. Since no gas was extracted, these values are based on the SOFC system model, that is similar to the one used by Wagner et al. [18]. A higher AOR leads to higher $S/CH4$ and O/C ratios, and thus reduces the carbon deposition risk in the reformer and the SOFC anode.

- During the startup phase of the SOFC system, water vapor can be supplied from an external source (electrical evaporator) to the steam reformer (stream 22). However, the external steam is no longer necessary during operation with the AOR. A final version would need an internal water storage tank, which could be filled during nominal operation and an additional start-up burner, which can heat the SOFC stack and the evaporator during the startup procedure. The evaporator could supply steam to the steam reformer (stream not shown in Figure 2) until the AOR is sufficiently high.

- The FTU and the SOFC stack are placed in two separate electrical ovens (solid green lines) at different temperatures. The SOFC stack, fuel and air preheaters (stream 3 and 24, respectively), steam reformer, the burner, and the HEX downstream of the burner are in a hot box

at 710 °C. Thus, no internal heat recovery was implemented, since the anode and cathode gas preheating was realized with static HEXs. The FTU and the RR measurement devices (V1 and V2) are at 195 °C. The electricity of these two ceramic ovens (stream 30 and 32) would thus need to be accounted as auxiliary power to calculate the SOFC system electrical net efficiency. In a final realization, all previously mentioned components would be placed in an insulated hot box, that is not actively heated.

- The SOFC stack has a gross DC power of 6 kW_e; however, the FTU was originally designed for a 10 kW_e system.

- The blade tip clearance in the AOR fan is 0.15 mm instead of the original design value of 0.05 mm for risk mitigation. The fan blade tip clearance has a significant impact on the achievable pressure rise at a given mass flow rate. During the experiments presented in this article, the maximum fan total-to-total pressure rise was 64.5 mbar for a fan mass flow rate of 2.7 $kg\,h^{-1}$ and a rotational speed of 165 krpm. However, the fan with the design tip clearance of 0.05 mm is expected to rise the pressure by 70 mbar at the design AOR mass flow rate of 4.9 $kg\,h^{-1}$ and the design rotational speed of 175 krpm. [16]

- A manually-operated ball valve at the fan outlet prevents the fluid from bypassing the SOFC stack, e.g., the flow direction of streams 7, 6, and 5 (in Figure 3) is reversed during the startup phase. This could be replaced with a more simple check valve in a final version.

- The anode off gas (stream 9) and the cathode off-gas (stream 25) were

mixed in the burner; hence, the air-fuel equivalence ratio in the burner is much higher than the stoichiometric value. This leads to a lower water vapor molar fraction in the anode off-gas, to less condensed water, to a lower heat recovery in the condenser (stream 10), and thus to a lower utilization ratio. Keeping the stream 9 and 25 separate is thus favorable for increased condensation of water, increased utilization ratio and better control of the flame temperature [20]. Additionally, ambient air is mixed into the burner (stream 27) to control the burner outlet temperature to 730 °C.

- The non-recirculated anode off-gas (stream 8-11) is first condensed, burned, and recondensed. The reverse order (first burning and then condensing) reduces the heat losses of the HEXs.

- The cathode air mass flow rate is kept constant at $55.8\,\mathrm{kg\,h^{-1}}$ for all operating points. The electrical net efficiency is thus not optimized, since the mass flow rate, and thus the cathode fan power consumption (stream 31 in Figure 3) could be lowered for the part-load experiments.

- The evaporator is electrical (stream 29), and thus the FTU and the SOFC are not thermally coupled, i.e., the HEX downstream of the burner does not provide heat to the evaporator.

- The turbine and the SOFC water systems are not coupled. The pump (KNF SIMDOS10) draws deionized water from an external tank (stream 15 in Figure 3); hence, a water treatment system is not necessary. The expanded steam in the turbine leaves the system via chimney (stream

19). The condensed water from the SOFC system (stream 11 and stream 12) is sent to drain.

- Due to the proof-of-concept nature of the presented setup, no automation was included; hence, a constant on-site surveillance of the entire system was necessary.

Figure 4 shows a) a digital image of the oven that contains the FTU, b) a digital image of the two Venturi nozzles that measure the RR, and c) a photo of the implemented FTU test rig without the oven cover.

Anode off-gas cooling: On the anode side, the off-gas exits the SOFC at a temperature of up to 800 °C. Since the FTU is designed for an operational temperature of 200 °C, an HEX precools the off-gas (stream 4, not shown in Figure 3) with ambient air to 200 °C. The off-gas is then conducted to the fan inlet in corrugated pipes that are exposed to the FTU oven atmosphere, thus adapting the gas temperature to the FTU temperature. A constant temperature at the fan inlet is guaranteed, favoring stable operation of the FTU.

Measurement of the RR: Downstream of this anode outlet HEX, the off-gas enters a custom-made double Venturi nozzle in accordance with ISO 5167-4 norm [21], as shown in Figure 4 b). The entrance is stream 4 (anode off-gas), the exit to the burner is stream 8, and the exit to the AOR fan is stream 5. Thus, the burner mass flow rate is measured in the Venturi 1 (V1) and the AOR mass flow rate in Venturi 2 (V2) as shown in Figure 3. This design is advantageous, since the temperatures, pressures, and gas compositions, and

thus the densities are in both Venturi nozzles identical. Thus, the RR

$$RR = \frac{\dot{n}_5}{\dot{n}_4} = \frac{1}{\frac{CD_{V1}\left(Re_{d_h,V1}\right)}{CD_{V2}\left(Re_{d_h,V2}\right)}\sqrt{\frac{\Delta p_{V1}}{\Delta p_{V2}}} + 1} \tag{11}$$

is a function of the Venturi nozzle differential pressures (Δp) between the static pressure measurement at the inlet and at the throat pressure tap (+ and -, respectively, in Figure 4 b). The discharge coefficient (CD) is a function of the Reynolds number based on the throat hydraulic diameter (Re_{d_h}), assuming a similar fluid density and geometry for both Venturi nozzles. A 1.5 mm diameter k-type thermocouple (red point in Figure 4 b) measures the fluid temperature downstream of Venturi nozzle 1. The pressure tap at the nozzle throat (- in Figure 4 c) measures the differential pressure with respect to the ambient. With these two variables and the ambient pressure, it is possible to calculate the fluid density, viscosity, and velocity. This allows to compute the Reynolds numbers and the discharge coefficients (CD_{V1} and CD_{V2}). However, the exact fluid composition remains unclear and is estimated with an SOFC stack model, similar to the one used by Wagner et al. [18]. The estimated anode off-gas fluid compositions and densities are listed in Tables 3 and 5. An off-gas extraction would be a more accurate option. According to the ISO 5167-4 norm [21], the Venturi nozzle discharge coefficient is constant for high Reynolds numbers (above 2×10^5). However, for lower Reynolds numbers, it drops with decreasing Reynolds number. Since the Re_{d_h} may drop significantly below 15 000 during the tests, which strongly affects the discharge coefficient, and due to the fact that the Venturi nozzle area deviates from the norm, the nozzles were calibrated in-house.

Measurement of turbomachinery parameters: The turbomachinery

power

$$P = M\omega \tag{12}$$

is typically measured with the shaft torque (M) and the angular velocity (ω). Wagner et al. [16] listed several reasons why the shaft torque measurement is challenging for this small-scale application. They introduced a measurement setup for the determination of the fan power and efficiency, which is also used in this work. It is based on the measurement of the inlet and outlet enthalpies ($\dot{m}h_t\left(p_t, T_t\right)$), assuming an adiabatic system and a leakage mass flow rate between the turbine and the fan of 0.

$$P_{fan} = \dot{m}_{fan}\left(h_{t,fan,out} - h_{t,fan,in}\right) \tag{13}$$

$$P_{turb} = \dot{m}_{turb}\left(h_{t,turb,in} - h_{t,turb,out}\right) \tag{14}$$

However, the assumption of an adiabatic system is not true, due to (1) heat conduction to the ambient and to the oven, (2) heat conduction between turbine and fan, and (3) heat conduction of the mechanical losses to the fan and turbine fluid domain. The first point can be tackled by insulating and decoupling the measurement sections inside the electrical oven with polytetrafluoroethylene (PTFE) tubing from the ambient, as suggested by Wagner et al. [16]. However, for the presented measurement campaign, this installation was not possible due the risk of CO leakage to the ambient. As alternative, the tubes (stream 6 in Figure 3) are heated to 180 °C with an electrical heating tape. This allows to measure the fan power and the

isentropic fan efficiency.

$$\eta_{fan} = \frac{P_{is,fan}}{P_{fan}} = \frac{\dot{m}_{fan}\Delta h_{tt,is,fan}}{P_{fan}} \tag{15}$$

$$= \frac{\dot{m}_{fan}\left(h_{t,is,fan,out}\left(p_{t,fan,out}, s_{fan,in}\right) - h_{t,fan,in}\right)}{P_{fan}} \tag{16}$$

It is the ratio of the isentropic fan power ($P_{is,fan}$) to the actual fan power (P_{fan}). The isentropic fan power is the product of the fan inlet mass flow rate ($\dot{m}_{fan}$) with the total-to-total isentropic specific enthalpy difference ($\Delta h_{tt,is,fan}$). This variable can be calculated with the total specifc enthalpy at the fan inlet ($h_{t,fan,in}$) and the total isentropic specific enthalpy at the fan outlet ($h_{t,,is,fan}$), which is a function of the total pressure at the fan outlet ($p_{t,fan,out}$) and the specific entropy at the fan inlet ($s_{fan,in}$). The isentropic turbine efficiency is calculated similarly.

$$\eta_{turb} = \frac{P_{turb}}{P_{is,turb}} = \frac{P_{turb}}{\dot{m}_{turb}\Delta h_{tt,is,turb}} \tag{17}$$

$$= \frac{P_{turb}}{\dot{m}_{turb}\left(h_{t,turb,in} - h_{t,is,turb,out}\left(p_{t,turb,out}, s_{turb,in}\right)\right)} \tag{18}$$

The mechanical efficiency of the shaft

$$\eta_{mech} = \frac{P_{fan}}{P_{fan} + P_{mech}} = \frac{P_{fan}}{P_{turb}} \tag{19}$$

is the ratio of the fan power (P_{fan}) to the turbine power (P_{turb}). The mechanical power loss

$$P_{mech} = P_{turb} - P_{fan} \tag{20}$$

is defined as the difference between the turbine and the fan power. It can be indirectly measured with run-out tests. In this article an analytical windage loss model by Demierre et al. [22] is used. They compared the model to rotor

run-out measurements of a micorcompressor-turbine unit and it correlated within a $\pm 10\,\%$ band. The model is based on the measured shaft rotational speed, the bearing temperature, and the housing pressure.

The FTU efficiency is the product of the fan efficiency (η_{fan}, eqs. (15) and (16)), the turbine efficiency (η_{turb}, eqs. (17) and (18)), and the mechanical shaft efficiency (η_{mech}, eq. (19)). Using the definitions of the isentropic fan power from eq. (16) and the isentropic turbine power from eq. (18), it is thus possible to calculate the total FTU efficiency with the measured inlet data (mass flow rates, temperatures, and pressures) and the measured outlet pressures.

$$\eta_{FTU} = \eta_{fan}\eta_{mech}\eta_{turb} = \tag{21}$$

$$\eta_{FTU,2} = \frac{\dot{m}_{fan}\left(h_{t,is,fan,out}\left(p_{t,fan,out}, s_{fan,in}\right) - h_{t,fan,in}\right)}{\dot{m}_{turb}\left(h_{t,turb,in} - h_{t,is,turb,out}\left(p_{t,turb,out}, s_{turb,in}\right)\right)} \tag{22}$$

Considering an accurate measurement and an accurate mechanical loss model, the FTU efficiency definition of eq. (21) based on the multiplication of the component efficiencies is equal to the efficiency definition in eq. (22) based on the turbomachine inlet conditions and the outlet pressures. The authors assume that the definition from eq. (22) is more accurate to measure than the definition in eq. (21), since it does not use the measured fan and turbine outlet temperatures, which can be strongly affected by heat conduction. The turbine power and efficiency measurement is more challenging than the fan measurement, since the turbine surface-to-volume ratio, the velocity (turbine choked), and the temperature difference are higher. The authors therefore propose a corrected turbine efficiency and power based on the measured FTU efficiency (eq. (22)), the measured fan efficiency (eq. (16)), and the

analytically estimated mechanical efficiency (eq. (19)).

$$\eta_{turb,corr} = \frac{\eta_{FTU,2}}{\eta_{mech}\eta_{fan}} \tag{23}$$

$$P_{turb,corr} = P_{turb}\frac{\eta_{turb,corr}}{\eta_{turb}} \tag{24}$$

Another variable that can be measured during the experimentation is the turbine reaction.

$$\delta = \frac{p_{rs} - p_{amb}}{p_{turb,in} - p_{amb}} \tag{25}$$

It is calculated with the measured turbine rotor-stator static pressure (p_{rs}), the ambient pressure ($p_{amb} = 0.98\,\text{bar}$), and the turbine inlet static pressure ($p_{turb,in}$).

Data acquisition: The FTU and the SOFC measurement data are acquired on two different systems: the SOFC system has a sampling rate of 0.33 Hz and the FTU system of 1 Hz. The FTU rotational speed was measured with an optical probe (sampling rate of 50 kHz). The data points in Tables 2 to 5 correspond to the averaged values over a time frame of 15 s.

4. Results and analysis

The steam-driven FTU was successfully coupled with a prototype 6 kW_e SOFC stack provided by the company SOLIDpower. "SOLIDpower cells are standard Ni-YSZ anode-supported cells, on which an electrolyte (YSZ), a barrier layer (GDC), LSCF:GDC composite cathode, LSCF, and current collector layer are deposited and sintered. (...) The cell layers thicknesses are 240 µm for the anode support, 10 µm for the thin electrolyte, 68 µm for the barrier layer, and 60 µm for the bilayer cathode, respectively." [23]

Three different measurement campaigns were carried out: (1) the SOFC stack

without AOR, (2) coupling procedure of the SOFC stack and the FTU, and (3) the characterization of the coupled system at different loads and different FUs.

The measured electrical gross DC efficiency (eq. (2)) was 66 % in part load (4.5 kW_e) and 61 % in full load (6.4 kW_e) for a global FU of 85 %. The global FU was measured.

$$f_{u,global} = \frac{I}{z_e \boldsymbol{F}} \frac{z_{layer}}{\dot{n}_{1,CH4}} \tag{26}$$

It is controlled with the SOFC load and it is measured with the SOFC current (I) and the fuel molar flow rate ($\dot{n}_{1,CH4}$), assuming steam reforming of methane ($z_e = 8$) and a stack with 60 layers ($z_{layer} = 60$). The local FU is a function of the measured global FU in eq. (26) and of the measured RR in eq. (11).

$$f_{u,local} = f_{u,global} \frac{1 - RR}{1 - RR f_{u,global}} \tag{27}$$

The anode off-gas (stream 8 in Figure 3 and Figure 2) contains water vapor, as well as unused hydrogen. Thus, the maximum molar flow rate of condensable water vapor

$$\dot{n}_{water} = 2\dot{n}_{1,CH4} \tag{28}$$

is a function of the fuel molar flow rate ($\dot{n}_{1,CH4}$). The excess water ratio (EWR)

$$EWR = \frac{\dot{n}_{water}}{\dot{n}_{15}} \tag{29}$$

is a function of the measured turbine steam molar flow rate ($\dot{n}_{15}$, stream 15 in Figures 2 and 3). It is an indicator, whether enough water is available in

the anode off-gas to propel the turbine As a result, there are three different cases.

- $EWR > 1$: The steam molar flow rate through the turbine is lower than the maximum molar flow rate of condensable water vapor. Thus, no water vapor needs to be recirculated to the condenser (stream 14 and 20 in Figure 2 are zero) and the entire water vapor leaves the system at stream 21. The water recirculation ratio

$$RR_{water} = \frac{\dot{n}_{15}}{\dot{n}_{12}} \tag{30}$$

  is the ratio of the molar flow rate of stream 15 to stream 12 (both in Figure 2) is therefore smaller than 1. Thus, some water leaves the system at stream 13.

- $EWR = 1$: Stream 13, 14, and 20 in Figure 2 are zero, i.e., the condensed water within the system is equal to the turbine steam molar flow rate.

- $EWR < 1$: The steam molar flow rate through the turbine is higher than $\dot{n}_{water}$; hence, part of the steam through the turbine needs to be recirculated. The steam recirculation ratio

$$RR_{steam} = \frac{\dot{n}_{20}}{\dot{n}_{19}} \tag{31}$$

  is the ratio of the molar flow rate of stream 20 to stream 19 (both in Figure 2) is thus greater than 0. As alternative, fresh water can be supplied via stream 14.

The cathode air mass flow rate was kept constant at 55.846 kg h^{-1} for all experiments (experiment c0 to c12 and 1 to 18), corresponding to an excess air ratio

$$EAR = \frac{\dot{n}_{23,air} 0.21}{2\dot{n}_{1,CH4}} \tag{32}$$

of 4.4 for the coupling procedure (methane mass flow rate of 0.7417 kg h^{-1}). The auxiliary powers were not measured. Thus, an exact calculation of the electrical net efficiencies was not possible and Tables 2 and 4 only present the electrical gross DC efficiencies (eq. (2)).

Estimation of net power and efficiencies: However, the cathode fan power can be estimated with eq. (13) to 124 W (stream 31 in Figure 3), assuming the measured cathode fan pressure rise of 25 mbar, an inlet temperature of 25 °C, a fan isentropic efficiency of 60 %, a mechanical efficiency of 50 %, and an electrical efficiency of 90 % (total efficiency of 27 %). The maximum power of the KNF SIMDOS10 pump is 12 W (24 V and 0.5 A) and it was operated between 33 % and 23 % of the maximal mass flow rate (6 kg h^{-1}). The pump power is therefore estimated to be less than 12 W (stream 28 in Figure 3). Assuming another 15 W for the burner fan (stream 33 in Figure 3) and 50 W for controllers and communication, the estimated auxiliary power sums up to 201 W. The electrical net DC efficiency (eq. (3)) would therefore be between 2.0 % points (experiment 1-4 in Table 4) to 3.9 % points (experiment 15-18 in Table 4) lower than the stated electrical gross DC efficiency. Assuming an DC/AC converter efficiency of 95 %, the electrical net AC efficiency (eq. (4)) would therefore be between 4.6 % points and 7.1 % points lower.

Cell potential: Figure 5 shows the measured cell potentials and the current of the 6 kW_e SOFC stack at the design-point with four different global FUs. The four numbers (①, ②, ③, and ④) in Figure 5 correspond to the four experiments listed in Tables 4 and 5 (experiment number 1, 2, 3, and 4). The global FU corresponds to 0.7, 0.75, 0.8, and 0.85, respectively. The six cell potential curves were obtained from six different measurement locations in the stack, each averaged over 10 cells (total cell number is 60). During experiment 1 (global FU of 0.7), the difference between the maximum measured cell potential (0.819 V) and the minimum measured cell potential (0.807 V) was 0.012 V, suggesting a homogeneous distribution of the fuel and similar cell efficiencies. The cell voltage efficiency (cell potential divided by the reversible potential) was 79 % and 78 %, respectively, at this operational point. The cell potential dropped to 0.769 V and 0.737 V, respectively, for experiment 4 (global FU of 0.85). This is equal to a cell voltage efficiency of 74 % and 71 %, respectively. Since the difference between the maximum and minium cell potential (0.032 V) was relatively high at this operational point, the SOFC stack was only operated for several minutes at a global FU of 0.85. In order to protect the prototype SOFC stack, a global FU higher than 0.85 was not investigated.

Coupling procedure: Tables 2 and 3 represent the evolution of the results during the transition phase of the coupling procedure between the FTU and the SOFC stack. The experiments c0 to c12 were conducted chronologically in 12 discrete steps. The coupling procedure was as follows:

1. Increase the mass flow rate of the pump, what leads to a higher fan

rotational speed, and thus to a higher AOR

2. Wait until the AOR fan and the SOFC stack are stationary (25 to 35 minutes)
3. Decrease the external steam supply for the reformer (stream 22 in Figure 3)
4. Repeat the step 1-3 until the external steam supply is zero.

During the first experiment (c0), the steam for the reforming process was exclusively supplied from an external electrical evaporator (stream 22). This steam injection was then gradually reduced from $1.74\,\mathrm{kg\,h^{-1}}$ to 0, while the RR was increased from 0 (c1) to 47 % (c12). This RR was realized with turbine steam mass flow rates of $1.4\,\mathrm{kg\,h^{-1}}$ and $2.0\,\mathrm{kg\,h^{-1}}$, respectively, which corresponded to turbine total-to-total pressure ratios of 1.5 and 1.8, respectively, and a shaft rotational speeds of 148 krpm and 170 krpm, respectively.

Before coupling the AOR fan with the stack (experiment c0), the fan outlet total pressure was adjusted to be slightly above the reformer inlet total pressure. After the valve was opened (ball valve in Figure 3), the AOR started, which resulted in a slight drop of the total-to-total fan pressure rise from 50 mbar (experiment c0) to 46 mbar (c1). Since the anode mass flow rate increased with increasing RR, the fan total-to-total pressure rise increased from 46 mbar (experiment c1) up to 62 mbar (c10). For the last three coupling steps (experiments c10, c11, and c12), the turbine inlet steam mass flow rate was constant ($1.98\,\mathrm{kg\,h^{-1}}$). The anode off-gas mass flow rate decreased from $5.0\,\mathrm{kg\,h^{-1}}$ (experiment c10) to $4.9\,\mathrm{kg\,h^{-1}}$ (c12); hence, the fan total-to-total pressure rise decreased from 62 mbar (c10) to 59 mbar (c12).

During the coupling process, the methane mass flow rate and the global FU were maintained constant at $0.74\,\mathrm{kg\,h^{-1}}$ and 0.7, respectively. The local FU decreased from 0.7 (experiment c0) to 0.55 (c12), since the RR gradually increased. The hydrogen molar mass fraction increased from 20.3 % (c0) to 28.6 % (c12), due to the AOR and the decreasing steam-to-methane ratio from 2.1 (c0) to 1.1 (c12). As a result the mean cell voltage increased from 0.797 V (c0) to 0.813 V (c12); the electrical power output and the electrical gross DC efficiency increased by $0.11\,\mathrm{kW_e}$ and 1.1 % points, respectively. However, the reformer and anode inlet were operating closer to carbon formation, since the calculated oxygen-to-carbon ratio decreased from 2.1 (c0) to 1.3 (c12). The calculated external reforming fraction decreased from 95 % (c0) to 84 % (c12), suggesting a higher quenching effect in the SOFC stack. Table 2 also lists the EWR as defined in eq. (29). For experiment c0 to c4, the EWR is above 1, suggesting that theoretically enough water vapor is available in the anode off-gas. However, the actual available water vapor is lower, since the burner has an efficiency lower than 100 % and a fraction of the water vapor can not be condensed. This depends on the anode off-gas composition (e.g., excess air ratio in the burner) and on the condensing temperature. In the final system, the actual EWR would therefore be lower. For experiment c5 to c12, part of the turbine exhaust needs to be recirculated to the condenser, as indicated by the minimum steam recirculation ratio.

$$RR_{steam,min} = 1 - EWR \tag{33}$$

Characterization: Figure 6 and Tables 4 and 5 summarize the characterization of the $6\,\mathrm{kW_e}$ SOFC stack coupled to the steam-driven AOR fan. Each number in Figure 6 corresponds to an experiment listed in Tables 4

and 5. The system was characterized at different loads, corresponding to different methane mass flow rates (60 layers a 4 cells with an active area of $80\,\mathrm{cm}^2$). The experiments were conducted chronologically from experiment 1-18.

- 100 % load ($0.742\,\mathrm{kg\,h}^{-1}$): experiment 1-4
- 92 % load ($0.679\,\mathrm{kg\,h}^{-1}$): experiment 5-10
- 66.7 % load ($0.496\,\mathrm{kg\,h}^{-1}$): experiment 11-14
- 50 % load ($0.372\,\mathrm{kg\,h}^{-1}$): experiment 15-18

The current density at 92 % load and a FU of 0.85 corresponds to the current density of the BlueGEN produced by SOLIDpower ($0.40\,\mathrm{A\,cm}^{-2}$). For each load case, four different global FUs (i.e., 0.7, 0.75, 0.8, and 0.85) were investigated. The turbine inlet temperature was maintained constant (220 °C ± 5 °C), as well as the fan inlet temperature (195 °C ± 5 °C). The turbine steam mass flow rates were constant at $1.98\,\mathrm{kg\,h}^{-1}$, $1.74\,\mathrm{kg\,h}^{-1}$, $1.50\,\mathrm{kg\,h}^{-1}$, and $1.38\,\mathrm{kg\,h}^{-1}$ for the 100 %, 92 %, 66.7 %, and 50 % load cases, respectively. For the 92 % load case, turbine steam mass flow rates of $1.98\,\mathrm{kg\,h}^{-1}$ (FU of 0.7, 0.75, 0.8, and 0.85) and $1.74\,\mathrm{kg\,h}^{-1}$ (FU of 0.8 and 0.85) were investigated.

For a fixed turbine mass flow rate, the resulting RR as stated in Equation (11) was not constant. It generally increases with increasing global FU, while the load, i.e., the fuel mass flow rate, is constant. It varies between 0.45 (experiment 9 in Figure 6 and Table 4) and 0.51 (experiment 7). A higher RR leads to a higher dilution of the anode inlet gas, to a lower cell Nernst potential, and thus to a lower system efficiency, but also to a higher O/C ratio,

and thus to a lower carbon deposition risk. The RR of experiment 7 and 8 was 0.51 (turbine inlet mass flow rate of 1.98 kg h^{-1}). It decreased to 0.44 and 0.45 for the experiment 9 and 10, respectively (turbine inlet mass flow rate of 1.74 kg h^{-1}). This leads to an increased electrical gross DC efficiency of 61.1 % and 63.0 %, respectively, as shown with the two blue up-pointing triangles in Figure 6. This is equal to an efficiency increase of 0.6 % points, compared to the two experiments with a RR of 0.51 (blue down-pointing triangles in Figure 6, numbered 7 and 8).

For a global FU of 0.85, electrical gross DC efficiencies of 61.5 %, 63.0 %, 65.8 %, and 66.9 % were reached for the 100 %, 92 %, 66.7 %, and 50 % load cases, respectively. This corresponds to a current density of 0.44 A cm^{-2}, 0.40 A cm^{-2}, 0.29 A cm^{-2}, and 0.22 A cm^{-2}, respectively.

Comparison to simulation model: Figure 6 also shows the simulated efficiencies (sim. eff.) with green dashed-dotted lines. The simulation model proposed by Wagner et al. [18] was used. The simulation does not model the stack quenching due to internal reforming. Within the presented experimental campaigns, the estimated internal reforming fraction was between 6 % (experiment 8) and 17 % (experiment 11). In a first approximation, the anode temperature is thus assumed as constant at the temperature of the electrical oven (710 °C). The experiments 1-3, 5-7, and 15-17 correlate well with the simulation model within ±0.4 % points. The change in load between the experiment 10 (92 % load) and experiment 11 (67 % load) was the highest. Thus, a certain amount of time is necessary until the stack cooled and was thermally stationary. The 50 min time between experiment 10 and 11 was not enough, wherefore the stack was not yet thermally stationary, and

the simulation underestimates the experiment 11, 12, and 13 by 0.7 % to 1 % point. For Experiment 4, 8, 10, and 18 with a FU of 85 %, the stack could not achieve a stationary thermal state due to the short operation time of a few minutes at this point. The simulation overestimates therefore the experiment by 0.7 % to 1.2 % points. The prediction by Wagner [17, 18] (electrical gross DC efficiency of 68.7 %) with a load of 84 %, a FU of 0.925 %, and a RR of 54 % is marked with a green hexagram.

Water management: For all the investigated operational points, the EWR was below 1, suggesting that the condensed water of the burner off-gas is not sufficient to drive the steam turbine. The EWR decreased from full load (0.84) to partial load (0.61), since the fuel inlet molar flow rate and thus the condensed water molar flow rate in the anode off-gas decreased. For all the experiments (1-18), part of the turbine exhaust would need to be recirculated to the condenser (stream 20 in Figure 2), as indicated by eq. (33).

Turbomachinery parameters: Figure 8 shows the total-to-total fan pressure rise and fan rotational speed for different loads and different fuel utilizations. The water vapor molar fraction in the anode off-gas, and thus the anode off-gas density increased with increasing FU. For a FU of 0.75, the anode off-gas density was $0.52\,\mathrm{kg\,m^{-3}}$ (for all four load cases), whereas it was $0.61\,\mathrm{kg\,m^{-3}}$ for a FU of 0.85 (increase by 16 %). The fan total-to-total pressure rise increases for higher fluid densities, or the fan rotational speed decreases if the pressure rise is constant, but the fluid density increases ($\Delta p_{tt} \propto \rho n_{rot}^2$). Thus, the shaft rotational speed decreased with increasing FU, although the anode pressure loss, and thus the fan pressure rise increased with increasing FU: For the 100 % load case, the pressure rise increased from

59.3 mbar at a FU of 0.70 to 64.3 mbar at a FU of 0.85 (8.5 %), whereas it was 6.0 %, 6.6 %, and 7.9 % for the 92 %, 67 %, and 50 % load case, respectively. Figure 9 shows the fan, shaft, and turbine power for different loads and different fuel utilizations. The fan and turbine power are calculated with eqs. (13) and (14), respectively. Figure 9 also indicates the error, since the expression $P_{turb} - P_{fan} - P_{mech}$ has to be 0. This error is between −7.3 W to −6.2 W for experiments 1-8, −2.6 W for experiments 9-10, and +0.6 W to +1.5 W for experiments 11-18. A corrected turbine power (eq. (24)) is stated, which is 28 W for experiments 1-8.

Figure 10 shows the fan, shaft, and turbine efficiency for different loads and different fuel utilizations. The fan, shaft, and turbine efficiencies are calculated according to eq. (16), eq. (19), and eq. (18), respectively. Since the authors consider the measured fan power as more accurate, the mechanical efficiency is calculated based the fan power. Figure 10 also compares the FTU efficiency 1 ($\eta_{FTU,1}$) and 2 ($\eta_{FTU,2}$) according to eq. (21) and eq. (22), respectively, which should be identical. The authors consider $\eta_{FTU,2}$ as more accurate, since it depends on the inlet conditions and the outlet pressures, which are not influenced by heat conduction. The corrected turbine efficiency (eq. (23)) is based on the $\eta_{FTU,2}$ efficiency definition. Typically, the turbine reaches the highest efficiency at the design rotational speed of 175 krpm: the turbine efficiency should increase while approaching the design speed. Thus, the corrected turbine efficiency (light dotted line) is more plausible than the actual measured turbine efficiency (dotted line), that decreases with increasing rotational speed.

For experiment 9 and 10, the FTU efficiency 2 is higher than the FTU effi-

ciency 1 (1.2 % points). For experiment 1-8, the difference is between +2.6 % and +2.8 % points and between −0.4 % and −0.8 % points for experiment 11-18. The lowest difference can be observed for experiment 14, which has a mechanical efficiency of 61 %, a fan efficiency of 37 %, and a turbine efficiency of 41 %.

The FTU efficiency is on the order of 11 % for experiments 1-10. The fan power is on the order of 17 W, the shaft mechanical loss on the order of 11 W, and the corrected turbine power on the order of 28 W for experiments 1-8. The fan mas flow rate of experiment 4 is with 2.75 $\mathrm{kg\,h^{-1}}$ the highest, and thus the closest to the design condition of 4.9 $\mathrm{kg\,h^{-1}}$. At this point, the measured fan efficiency is 48 %, the calculated mechanical efficiency is 61 %, and the turbine efficiency is estimated to be 40 %, leading to an FTU efficiency of 11.7 %.

Comparison to the stack without AOR: The SOFC stack was characterized at full load (fuel mass flow rate of 0.74 $\mathrm{kg\,h^{-1}}$) and for a global FU of 0 to 75 % without AOR (Figure 7). The point with a FU of 0.75 is marked with A in Figure 7. The operating point with AOR at full load and a global FU of 75 % corresponds to experiment 2 in Tables 4 and 5 and to the point marked with 2 in Figure 7. Thanks to the steam-driven AOR fan, the electrical gross DC efficiency (based on the LHV) was improved from 52.2 % to 57.4 % with the AOR, while the local FU decreased from 75 % to 61 %, suggesting a higher SOFC stack lifetime.

5. Conclusion

A novel anode off-gas recirculation fan was designed, manufactured, and experimentally coupled to a 6 kW_e SOFC system. This fan uses dynamic steam-lubricated bearings, more specifically herringbone-grooved journal and spiral-grooved thrust bearings that have proven to be reliable, even at temperatures up to 220 °C. Due to the high rotational speeds, the fan performance corresponds to the specified values, although the size is out of the common. The anode off-gas recirculation is driven by a small-scale, partial-admission (21 %), and low-reaction (15 %) steam turbine with a tip diameter of 15 mm, which allows for an explosion-proof operation. To the best of the authors' knowledge, this is the first proof-of-concept of such a steam-driven recirculation fan.

For a global fuel utilization of 75 % and a constant fuel mass flow rate, the electrical gross DC efficiency based on the fuel lower heating value was improved from 52 % to 57 % with the anode off-gas recirculation, while the local fuel utilization decreased from 75 % to 61 %, which is expected to significantly increase stack lifetime. For a global fuel utilization of 85 %, gross DC efficiencies of 66 % in part load (4.5 kW_e) and 61 % in full load (6.3 kW_e) were achieved with the anode off-gas recirculation.

For the first proof-of-concept, the steam-driven recirculation fan and the SOFC system were decoupled in terms of thermal and water management. A preliminary investigation indicates that the water content in the anode off-gas is at least 16 %, 12 %, and 26 % too low for the 100 %, 92 %, and 66.7 % load cases, respectively. Part of the turbine exhaust (at least 16 %, 12 %, and 26 %, respectively) therefore needs to be reused in the evaporator

that provides the steam to the turbine.

In a next step, the authors will decrease the recirculation fan tip clearance from the current 0.15 mm to 0.05 mm, which increases the fan efficiency and therefore reduces the steam consumption of the turbine. Another way to decrase the steam consumption is by increasing the turbine inlet temperature. In a future project, the authors want to couple the SOFC and the FTU systems completely in terms of water and thermal management.

6. Acknowledgment

The authors acknowledge the research grant from the Canton de Vaud under the "100 millions de francs pour les énergies renouvelables et l'efficacité énérgetique".

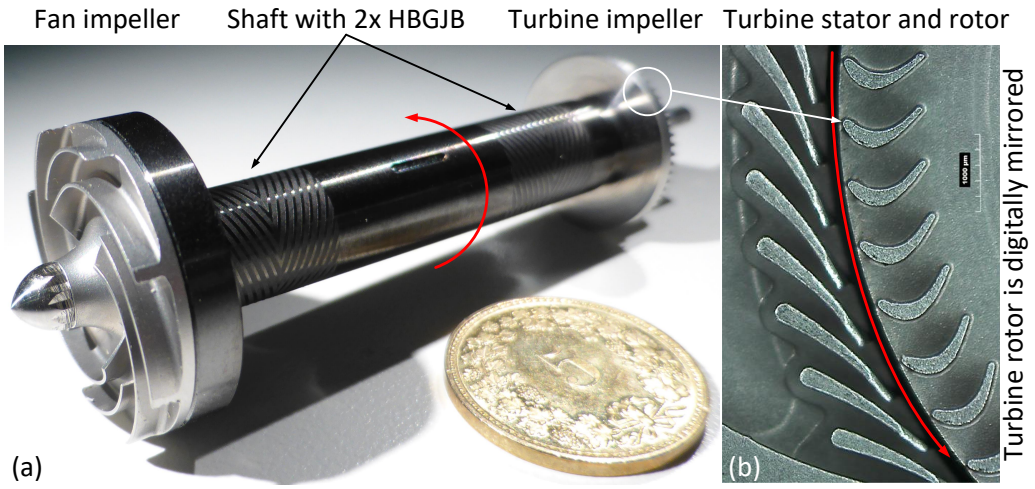

Figure 1: a) Fan-turbine unit with the radial fan impeller (left side), shaft with diamond-like carbon coating and two herringbone-grooved journal bearings (HBGJBs), radial-inflow turbine (right), and a comparison to a Swiss five cents coin (diameter at 17 mm). The direction of rotation is shown with a red arrow in figure a) and b). Figure b) shows a zoom of the turbine rotor and stator blades (radial blade chord of 1 mm). The turbine blades are digitally mirrored, since turbine rotor and stator are normally mounted facing opposites directions.

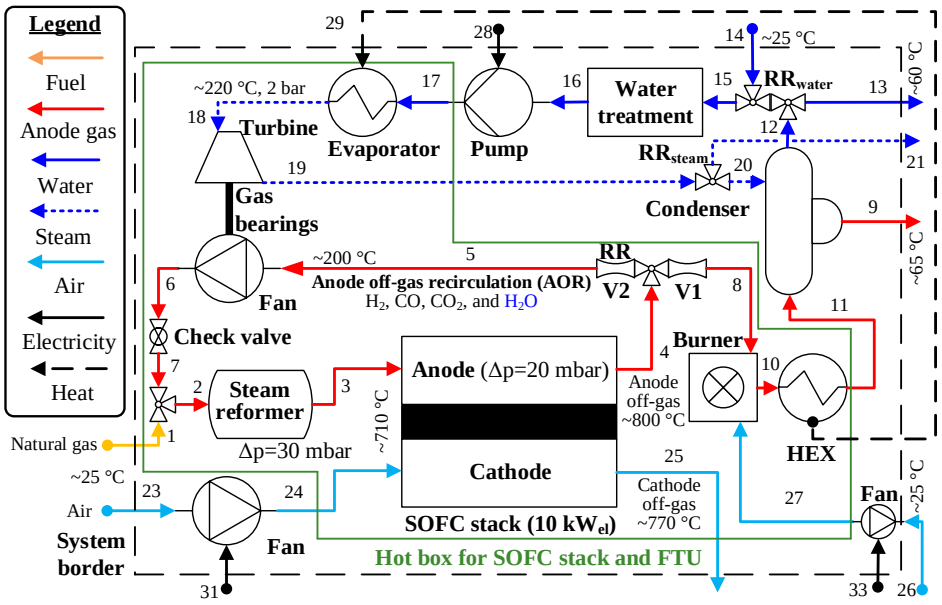

Figure 2: Natural-gas-fueled solid oxide fuel cell system with steam reforming, featuring a novel a steam-driven and steam-lubricated anode off-gas recirculation fan (Figure 1). One portion of the anode off-gas is sent to the burner (stream 8), a second portion is recirculated (stream 5) to the reformer and provides water vapor for the steam reforming reaction. The pressure loss of the anode off-gas recirculation loop, the reformer, and the anode is compensated with the anode off-gas recirculation fan, propelled by a steam turbine. This turbine is driven with evaporated and pumped water from the condensed anode off-gas. Heat recovered from the burner exhaust (stream 10) is recovered for the evaporator.

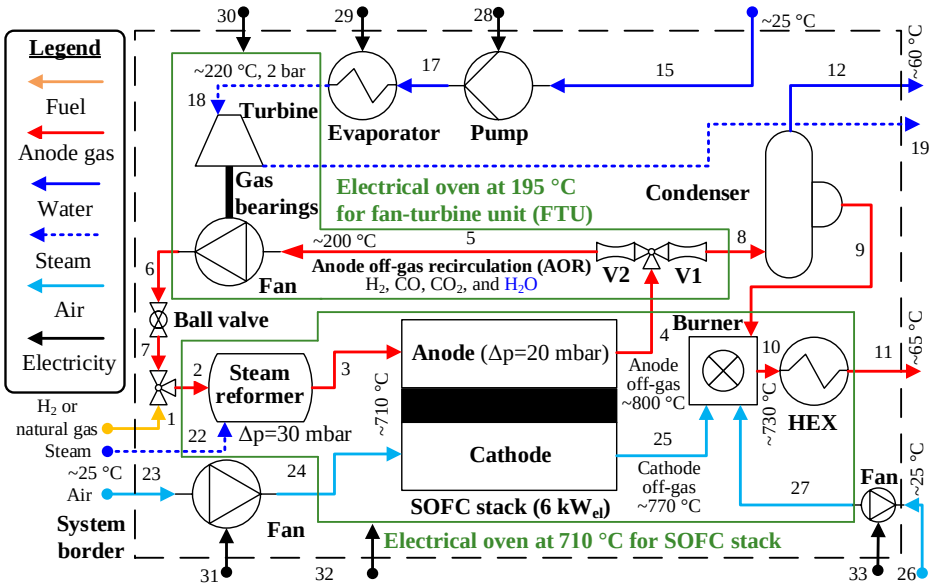

Figure 3: Realization of a solid oxide fuel cell system with steam-driven anode off-gas recirculation fan (Figure 2) with the following simplifications: (1) The solid oxide fuel cell and the recirculator system are in two different electrical ovens at different temperatures (710 °C and 195 °C, respectively). (2) The two systems are not thermally coupled, i.e., the evaporator is electrical. (3) The water is not drawn from the condensed anode off-gas, but from a tank with deionized water.

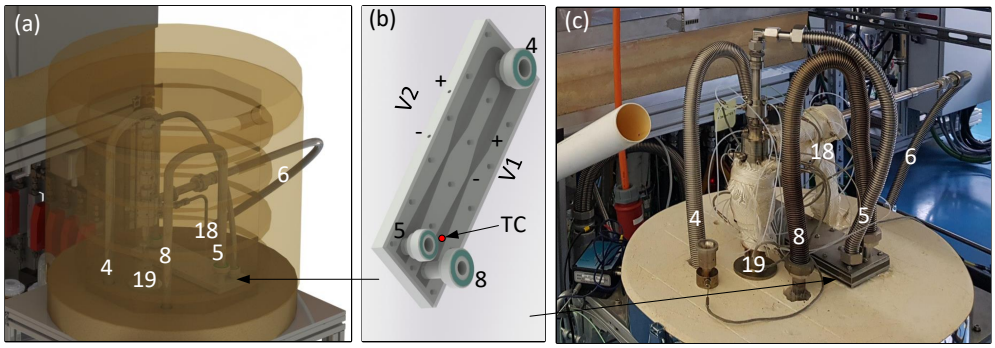

Figure 4: FTU test rig coupled with the SOFC: a) a digital image with mounted oven, b) the two Venturi nozzles for the recirculation rate measurement, and c) a photo with unmounted oven for the FTU test rig section.

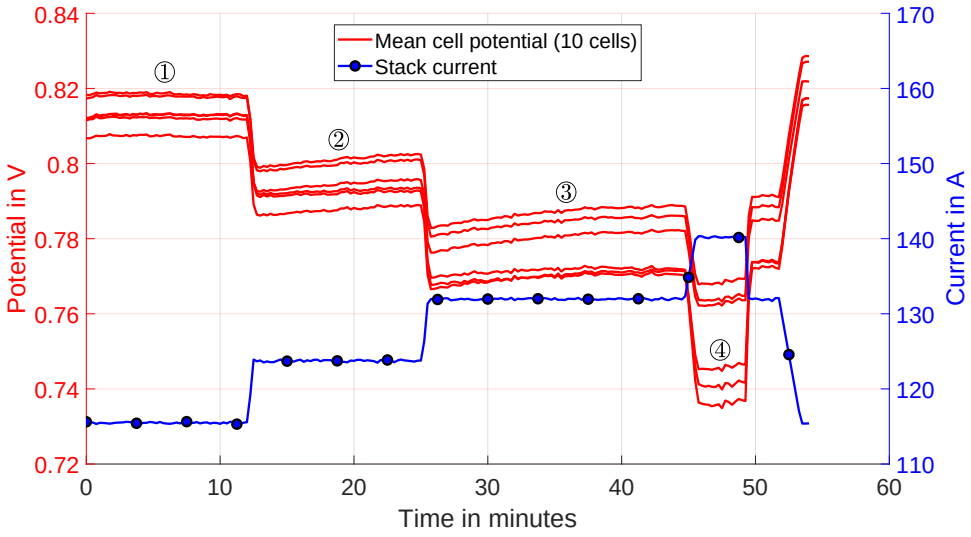

Figure 5: Measured cell potentials and total stack current for four experiments (1-4, as listed in Tables 4 and 5).

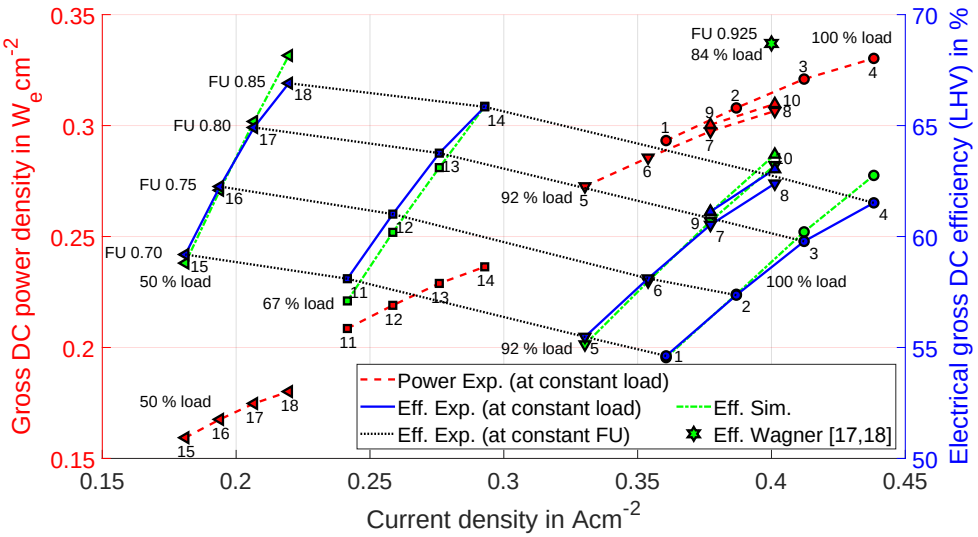

Figure 6: Electrical gross power density (60x4x80 cm^2 cells = 19 200 cm^2) and electrical gross DC efficiency (eff.) based on the fuel lower heating value (LHV) for the experiments (exp.) and the simulations (sim.) for an SOFC system with a steam-driven anode off-gas recirculation fan (recirculation ratios between 0.45-0.51). Different global fuel utilizations (0.85, 0.8, 0.75, and 0.70) and different loads (100 %, 92 %, 67 %, and 50 %), that correspond to different fuel mass flow rates were investigated. 100 % load corresponds to a fuel mass flow rate of 0.742 $\mathrm{kg\,h}^{-1}$. The numbers 1-18 correspond to the experiments in Tables 4 and 5.

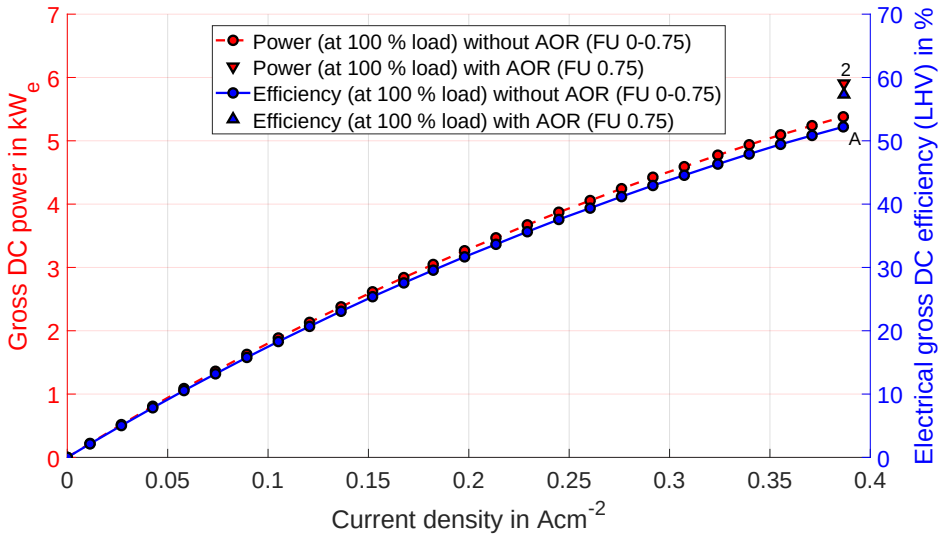

Figure 7: Electrical gross DC power and electrical gross DC efficiency based on the fuel lower heating value (LHV) for global fuel utilizations (FUs) from 0 to 0.75 at full load that corresponds to fuel mass flow rates of $0.742\,\mathrm{kg\,h^{-1}}$ without anode off-gas recirculation (AOR). Comparison of the point A to a system with a steam-driven AOR fan (FU of 0.75 and fuel mass flow rate of $0.742\,\mathrm{kg\,h^{-1}}$), which corresponds to the experiment 2 in Tables 4 and 5.

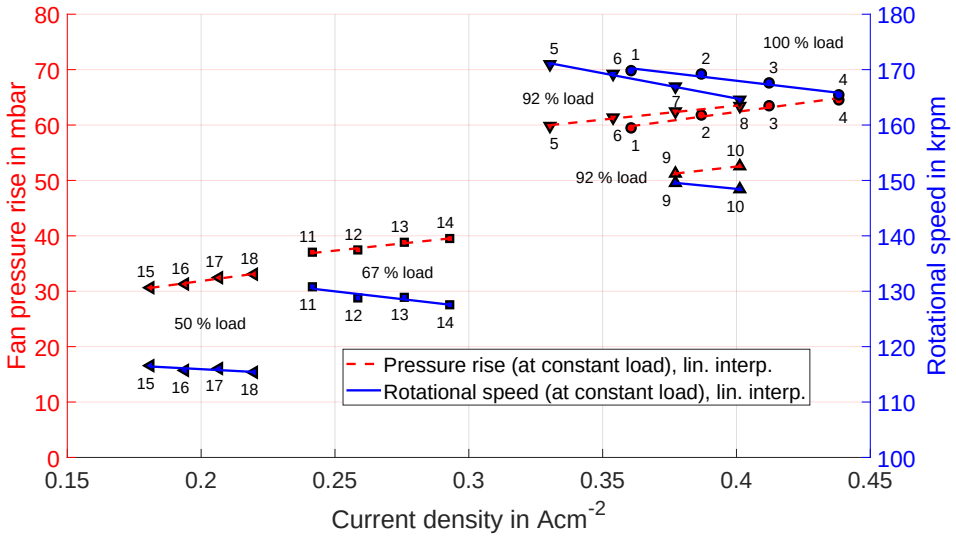

Figure 8: Total-to-total pressure rise and shaft rotational speed as a function of the SOFC stack current density. The numbers 1-18 correspond to the experiments in Tables 4 and 5.

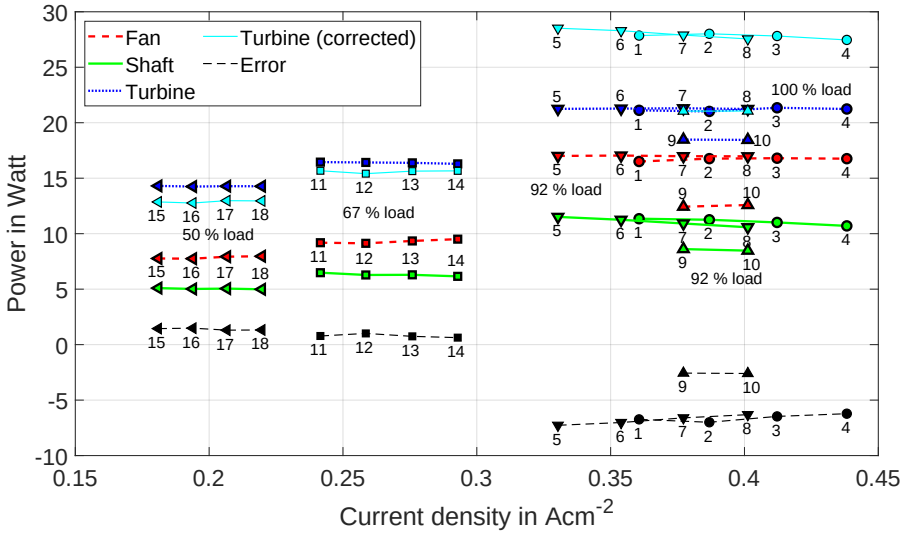

Figure 9: Fan and turbine power (calculated with measured inlet and outlet enthalpies, assuming an adiabatic system), shaft power (estimated with measured shaft rotational speed, bearing temperature, and housing pressure), resulting error ($P_{turb} - P_{fan} - P_{mech}$), and corrected turbine power (eq. (24)) as a function of the SOFC stack current density. The numbers 1-18 correspond to the experiments in Tables 4 and 5.

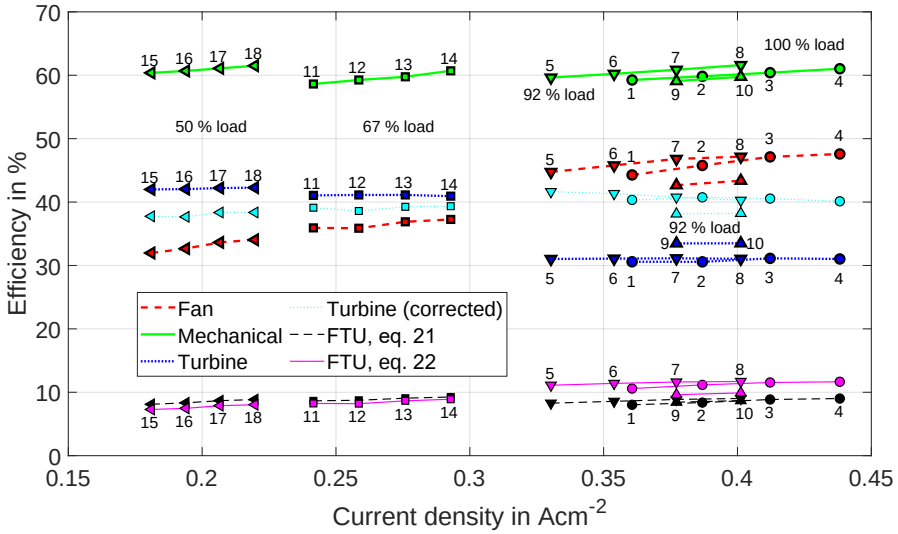

Figure 10: Fan and turbine isentropic total-to-total efficiency (calculated with measured inlet and outlet enthalpies, assuming an adiabatic system), shaft mechanical efficiency ($\frac{P_{fan}}{P_{fan}+P_{mech}}$, P_{mech} (estimated with measured shaft rotational speed, bearing temperature, and housing pressure), FTU efficiency according to eq. (21) and eq. (22), and corrected turbine efficiency (eq. (23)) as a function of the SOFC stack current density. The numbers 1-18 correspond to the experiments in Tables 4 and 5.

Table 1: Research (top), pre-commercial (middle), and commercial (bottom) solid oxide fuel cell systems with anode off-gas recirculation via ejector or fan. Non-formatted numbers are directly stated in the reference (measurement), *italic* numbers are estimated by the authors of the reference with a simulation, **bold** and underlined numbers are calculated and estimated, respectively, by the authors of this paper with the data available in the reference. A dash (-) indicates, that no information could be extracted from the reference.

Year of Ref.	Authors or Company	Cell Pot. V	DC power Gross kW_e	DC eff. Gross %	DC eff. Net %	AC eff. Net %	FU %	RR %	Current Density $A\,cm^{-2}$	Power Density $W\,cm^{-2}$	AOR Device[d]	Fuel[e]	Ref.
	Research												
2010	Noponen et al.	-	20	-	-	47.0	-	-	-	-	Fan (E)	LG	[1]
2011	Halinen et al.	**0.762**	9.8	**59.8**	**53.1**	50.0	82	61-63	**0.37**	**0.28**	Fan (E)	NG	[3, 4]
2012	Powell et al.	**0.698**	1.9	62.7	55.8	-	93	86	**0.21**	**0.15**	Fan (EM)	CH4	[8]
2012	Powell et al.	**0.683**	2.6	56.6	48.2	-	86	86	**0.30**	**0.21**	Fan (EM)	CH4	[8]
2013	Dietrich et al.	**0.690**	0.9	55.0	-	-	**86**	***42-56***	**0.16**	**0.11**	Ejector (F)	C3H8	[24]
2017	Peters et al.	**0.772**	2.5	64.0	***62.2***	*58.5*	90	74	**0.25**	**0.19**	Fan (EM)	CH4	[10]
2017	Peters et al.	**0.717**	4.0	60.5	***58.5***	*55.0*	90	73	**0.43**	**0.31**	Fan (EM)	CH4	[10]
2019	Exp. 8 in Table 4	0.820	3.5	66.9	*63.0*	*59.9*	85	49	0.22	0.18	Fan (SG)	NG	
2019	Exp. 14 in Table 4	0.764	5.9	62.4	*60.3*	*57.3*	85	51	0.40	0.31	Fan (SG)	NG	
	Pre-commercial												
2011	Siemens[a]	**0.616**	9.8	**38.0**	-	-	63	-	0.34	0.21	Ejector (F)	Mix	[2]
2013	AVL List	**0.735**	6.2	54.8	50.0[c]	-	78-81	-	**0.28**	**0.2**	Fan (EO)	NG	[13, 25]
2016	FuelCell Energy	**0.825**	55.8	61.0	56.0	***54.3***	85	-	**0.25**	**0.21**	Fan (E)	NG	[9]
2018	Bosch	-	10.0	70.0	-	-	-	-	-	-	Not disclosed	NG	[11]
2019	LGFCS Gen0	**0.800**	261.6	60.9	**57.6**	55.0	79	-	-	-	Ejector (F)	NG	[7]
2019	Convion C50	-	(58)[b]	-	-	>53	-	-	-	-	Not disclosed	NG	[26]
	Commercial												
2009	CFCL BlueGen	**0.839**	**1.7**	**69.3**	-	60.2	85	-	**0.40**	**0.34**	Pump	NG	[27]
2019	Energy Server 5	-	(250)[b]	-	-	53-65	-	-	-	-	Not disclosed	NG	[28]

[a] Data corresponds to the "POCD8R0" stack with fuel-driven ejector. The "POCD8R1" stack used an AOR fan. SOFC devolopment discontinued by Siemens

[b] AC net power

[c] "Efficiency" in [13] refers to the electrical net DC efficiency (personal communication with Stefan Megel, 25.10.2019)

[d] Anode off-gas recirculation device: Ejector (F): fuel-driven ejector, Fan (EM): electrically-driven fan with magnetic coupling, Fan (EO): electrically-driven fan with dynamic oil-bearings, Fan (E): electrically-driven fan, Fan (SG): steam-driven fan with gas bearings, or Pump: pumping of the condensed anode off-gas

[e] Fuel: LG (landfill gas), NG (natural gas), CH_4 (pure methane), C_3H_8 (pure propane), or Mix (91.5 % H_2, 6.5 % NG, and 2 % N_2)

Table 2: Coupling process of the FTU (steam-driven) with a 6 kW_e SOFC stack (60 layers a 4x80 cm^2 cells). The cathode air mass flow rate was maintained at 55.8 $kg\,h^{-1}$. The global fuel utilization was constant at 0.7. The turbine and fan inlet total temperatures were maintained at 220 °C ± 5 °C and at 195 °C ± 5 °C, respectively. The injected steam to the reformer was gradually replaced by anode off-gas recirculation (Part 1).

Exp.	$\dot{m}$ **CH_4** **$kg\,h^{-1}$**	$\dot{m}^{f}$ **H_2O** **$kg\,h^{-1}$**	**FU**[a] **local**	**RR**	U **stack** **V**	I **stack** **A**	P_{el} **stack** **kW_e**	$\eta_{el,gross}$[b] **(DC LHV)** **%**	T^{c} **anode** **°C**	T^{c} **cathode** **°C**	**O/C**[d] **before**	**S/CH4**[d] **reformer**	**External reforming fraction**[d]	EWR^{e}
c0	0.7417	1.740	0.7000	0.0000	47.80	115.4	5.516	53.51	743.0	730.0	2.089	2.089	0.9524	1.159
c1	0.7417	1.740	0.6792	0.0925	47.68	115.4	5.502	53.38	747.0	732.5	2.204	2.220	0.9577	1.159
c2	0.7417	1.667	0.6731	0.1174	47.69	115.4	5.503	53.39	751.5	736.5	2.226	2.262	0.9593	1.113
c3	0.7417	1.501	0.6669	0.1421	47.76	115.4	5.512	53.47	753.0	737.5	2.110	2.148	0.9525	1.070
c4	0.7417	1.334	0.6543	0.1888	47.84	115.4	5.521	53.56	753.5	738.0	2.071	2.127	0.9509	1.030
c5	0.7417	1.167	0.6429	0.2283	47.97	115.4	5.536	53.70	753.5	738.5	2.001	2.061	0.9468	0.993
c6	0.7417	1.000	0.6310	0.2672	48.06	115.4	5.546	53.80	753.5	738.5	1.919	1.972	0.9413	0.959
c7	0.7417	0.833	0.6173	0.3086	48.14	115.4	5.555	53.89	753.5	738.0	1.841	1.877	0.9349	0.927
c8	0.7417	0.667	0.6048	0.3441	48.24	115.4	5.567	54.01	753.0	737.5	1.745	1.747	0.9254	0.897
c9	0.7417	0.500	0.5875	0.3895	48.33	115.4	5.577	54.11	752.5	737.5	1.677	1.647	0.9156	0.869
c10	0.7417	0.334	0.5717	0.4279	48.43	115.4	5.589	54.22	752.0	737.0	1.590	1.505	0.9027	0.843
c11	0.7417	0.167	0.5509	0.4742	48.81	115.4	5.633	54.64	750.0	736.0	1.523	1.379	0.8905	0.843
c12	0.7417	0.00	0.5516	0.4740	48.79	115.4	5.630	54.62	750.0	736.0	1.325	1.026	0.8418	0.843

[a] Calculated with eq. (27)

[b] Caclulated with eq. (2)

[c] Mean temperature. The anode and cathode inlet temperatures were maintained at 710 °C ± 1 °C

[d] Oxygen-to-carbon ratio, steam-to-methane ratio, and external reforming fraction are estimated with experimental data

[e] According to eq. (29)

[f] Injected in the reformer for the steam reforming process (stream 22 in Figure 3)

[g] Experiment c12 is equal to experiment 1 in Tables 4 and 5

Table 3: Coupling process of the FTU (steam-driven) with a 6 kW_e SOFC stack (60 layers a 4x80 cm^2 cells). The cathode air mass flow rate was maintained at 55.8 $kg\,h^{-1}$. The global fuel utilization was constant at 0.7. The turbine and fan inlet total temperatures were maintained at 220 °C ± 5 °C and at 195 °C ± 5 °C, respectively. The injected steam to the reformer was gradually replaced by anode off-gas recirculation (Part 2).

Exp.	n_{rot}	$\dot{m}$	Π_{tt}[a]	δ[b]	$\dot{m}$[c]	ρ	**Molar fraction (γ_i) of the AOR**					Δp_{tt}[d]	η[e]
	shaft	**turbine**	**turbine**	**turbine**	**fan**	**AOR**	**CO_2**	**CO**	**H_2O**	**H_2**	**CH_4**	**fan**	**FTU**
	krpm	**kg h^{-1}**			**kg h^{-1}**	**kg m^{-3}**	**%**	**%**	**%**	**%**	**%**	**mbar**	**%**
c0	147.9	1.437	1.534	0.1427	0.000	0.4976	15.90	3.75	60.09	20.26	0.00	49.58	3.20
c1	145.5	1.437	1.528	0.1438	0.437	0.4995	15.98	3.67	60.43	19.92	0.00	46.40	3.14
c2	149.6	1.497	1.516	0.1450	0.559	0.5004	16.19	3.80	59.82	20.19	0.00	49.00	4.08
c3	151.9	1.557	1.532	0.1498	0.673	0.5018	16.69	4.14	58.32	20.86	0.00	50.40	4.72
c4	154.0	1.617	1.602	0.1442	0.906	0.5034	17.20	4.53	56.71	21.55	0.00	51.58	5.67
c5	156.8	1.677	1.643	0.1450	1.102	0.5053	17.74	4.98	54.99	22.29	0.01	53.04	6.49
c6	159.3	1.737	1.690	0.1421	1.298	0.5072	18.30	5.50	53.13	23.07	0.01	54.42	7.15
c7	163.1	1.797	1.720	0.1420	1.518	0.5094	18.88	6.11	51.11	23.89	0.01	56.47	8.09
c8	166.1	1.857	1.754	0.1407	1.696	0.5118	19.48	6.83	48.93	24.75	0.01	58.08	8.65
c9	169.7	1.917	1.798	0.1409	1.959	0.5145	20.11	7.66	46.54	25.68	0.01	60.04	9.61
c10	173.3	1.976	1.841	0.1388	2.176	0.5174	20.73	8.67	43.95	26.63	0.02	62.15	10.27
c11	170.0	1.976	1.826	0.1380	2.345	0.5204	21.34	9.89	41.11	27.62	0.03	59.32	10.63
c12	169.8	1.976	1.826	0.1375	2.352	0.5240	21.92	11.40	38.01	28.63	0.04	59.26	10.58

[a] Measured between turbine inlet and outlet

[b] Turbine reaction calculated with measured variables according to equation eq. (25)

[c] Mass flow rate calculation based on the estimated anode off-gas density and thus composition (γ_i). The exact gas composition was not measured

[d] Measured between fan inlet and outlet

[e] FTU efficiency calculated according to eq. (22)

[f] Experiment c12 is equal to experiment 1 in Tables 4 and 5

Table 4: 6 kW_e SOFC stack (60 layers a 4x80 cm^2 cells) with anode off-gas recirculation (FTU, steam-driven). The cathode air mass flow rate was maintained at 55.8 $kg\,h^{-1}$. The turbine and fan inlet total temperatures were maintained at 220 °C ± 5 °C and at 195 °C ± 5 °C, respectively (Part 1).

Exp.	$\dot{m}$ **CH_4** **$kg\,h^{-1}$**	**FU global**	**FU[a] local**	**RR**	U **stack V**	I **stack A**	P_{el} **stack kW_e**	$\eta_{el,gross}$[b] **(DC LHV) %**	T^c **anode °C**	T^c **cathode °C**	**O/C[d] before**	**S/CH4[d] reformer**	**External reforming fraction[d]**	EWR[e]
1	0.7417	0.70	0.5516	0.4740	48.79	115.40	5.630	54.62	750.0	736.0	1.325	1.026	0.8418	0.843
2	0.7417	0.75	0.6101	0.4797	47.76	123.80	5.913	57.36	751.0	736.0	1.438	1.179	0.8798	0.843
3	0.7417	0.80	0.6753	0.4816	46.72	131.90	6.162	59.78	755.5	738.5	1.541	1.318	0.9072	0.843
4	0.7417	0.85	0.7469	0.4805	45.22	140.20	6.341	61.52	756.5	739.5	1.634	1.445	0.9271	0.843
5	0.6789	0.70	0.5379	0.5018	49.52	105.70	5.234	55.48	750.0	737.0	1.403	1.146	0.8601	0.771
6	0.6789	0.75	0.5980	0.5047	48.41	113.30	5.482	58.11	748.5	735.5	1.513	1.301	0.8935	0.771
7	0.6789	0.80	0.6638	0.5067	47.31	120.70	5.710	60.53	748.5	735.0	1.621	1.458	0.9207	0.771
8	0.6789	0.85	0.7370	0.5059	45.84	128.40	5.886	62.39	748.5	735.0	1.72	1.599	0.9388	0.771
9	0.6789	0.80	0.6902	0.4461	47.78	120.70	5.767	61.12	752.8	738.5	1.427	1.143	0.8846	0.878
10	0.6789	0.85	0.7585	0.4481	46.32	128.40	5.947	63.03	752.9	738.4	1.523	1.268	0.9090	0.878
11	0.4959	0.70	0.5607	0.4567	51.80	77.30	4.004	58.10	732.7	727.4	1.277	0.9568	0.8275	0.744
12	0.4959	0.75	0.6224	0.4547	50.83	82.73	4.205	61.01	732.0	726.5	1.363	1.066	0.8619	0.744
13	0.4959	0.80	0.6854	0.4596	49.77	88.29	4.394	63.76	732.1	725.9	1.47	1.207	0.8942	0.744
14	0.4959	0.85	0.7538	0.4644	48.42	93.72	4.538	65.84	732.8	726.1	1.579	1.354	0.9202	0.744
15	0.3719	0.70	0.5507	0.4779	52.82	57.92	3.060	59.19	734.6	724.9	1.336	1.042	0.8462	0.606
16	0.3719	0.75	0.6114	0.4786	51.85	62.06	3.218	62.25	735.5	724.4	1.435	1.173	0.8799	0.606
17	0.3719	0.80	0.6744	0.4847	50.74	66.13	3.355	64.91	736.3	723.8	1.551	1.335	0.9094	0.606
18	0.3719	0.85	0.7449	0.4869	49.20	70.30	3.459	66.91	737.6	723.8	1.655	1.482	0.9307	0.606

[a] Calculated with eq. (27)

[b] Caclulated with eq. (2)

[c] Mean temperature. The anode and cathode inlet temperatures were maintained at 710 °C ± 1 °C

[d] Oxygen-to-carbon ratio, steam-to-methane ratio, and external reforming fraction are estimated with experimental data

[e] According to eq. (29)

Table 5: 6 kW_e SOFC stack (60 layers a 4x80 cm^2 cells) with anode off-gas recirculation (FTU, steam-driven). The cathode air mass flow rate was maintained at 55.8 $kg\,h^{-1}$. The turbine and fan inlet total temperatures were maintained at 220 °C ± 5 °C and at 195 °C ± 5 °C, respectively (Part 2).

Exp.	n_{rot}	$\dot{m}$	Π_{tt}[a]	δ[b]	$\dot{m}$[c]	ρ	**Molar fractions (γ_i) AOR**					Δp_{tt}[d]	η[e]
	shaft	**turbine**	**turbine**	**turbine**	**fan**	**AOR**	**CO_2**	**CO**	**H_2O**	**H_2**	**CH_4**	**fan**	**FTU**
	krpm	**kg h^{-1}**			**kg h^{-1}**	**kg m^{-3}**	**%**	**%**	**%**	**%**	**%**	**mbar**	**%**
1	169.8	1.976	1.826	0.1375	2.352	0.5240	21.92	11.40	38.01	28.63	0.04	59.26	10.58
2	169.2	1.976	1.823	0.1387	2.506	0.5518	24.00	9.33	42.64	24.02	0.02	61.58	11.16
3	167.6	1.976	1.819	0.1386	2.647	0.5801	26.00	7.33	47.32	19.34	0.01	63.24	11.54
4	165.5	1.976	1.817	0.1366	2.750	0.6078	27.93	5.40	52.07	14.60	0.00	64.29	11.65
5	171.0	1.976	1.817	0.1405	2.436	0.5241	21.95	11.37	37.98	28.66	0.04	59.59	11.11
6	169.2	1.976	1.817	0.1391	2.566	0.5516	24.02	9.31	42.62	24.04	0.02	61.10	11.40
7	167.0	1.976	1.816	0.1378	2.699	0.5796	26.00	7.33	47.32	19.34	0.01	62.19	11.62
8	164.6	1.976	1.816	0.1370	2.806	0.6074	27.93	5.40	52.07	14.60	0.00	63.17	11.70
9	149.6	1.737	1.717	0.1293	2.181	0.5790	26.00	7.34	47.33	19.33	0.01	51.07	9.61
10	148.4	1.737	1.715	0.1284	2.294	0.6064	27.93	5.40	52.07	14.60	0.00	52.39	9.90
11	130.8	1.497	1.562	0.1269	1.683	0.5226	21.92	11.40	38.01	28.63	0.04	36.94	8.24
12	128.8	1.497	1.558	0.1263	1.740	0.5502	24.00	9.33	42.64	24.01	0.02	37.34	8.20
13	128.9	1.497	1.556	0.1247	1.855	0.5777	25.99	7.34	47.33	19.33	0.01	38.72	8.65
14	127.6	1.497	1.555	0.1244	1.964	0.6052	27.92	5.42	52.08	14.59	0.00	39.38	8.90
15	116.6	1.378	1.505	0.1246	1.523	0.5222	21.92	11.41	38.02	28.62	0.04	30.55	7.29
16	115.7	1.378	1.501	0.1233	1.601	0.5497	23.99	9.33	42.65	24.01	0.02	31.20	7.47
17	116.1	1.378	1.500	0.1237	1.711	0.5774	26.00	7.33	47.33	19.34	0.01	32.34	7.88
18	115.4	1.378	1.499	0.1228	1.789	0.6050	27.93	5.41	52.07	14.59	0.00	32.97	8.03

[a] Measured between turbine inlet and outlet

[b] Turbine reaction calculated with measured variables according to equation eq. (25)

[c] Mass flow rate calculation based on the estimated anode off-gas density and thus composition (γ_i). The exact gas composition was not measured

[d] Measured between fan inlet and outlet

[e] FTU efficiency calculated according to eq. (22)

List of Acronyms

AC	alternating current
AOR	anode off-gas recirculation
DC	direct current
DLC	diamond-like carbon
EWR	excess water ratio
FTU	fan-turbine unit
FU	fuel utilization
HEX	heat exchanger
LHV	lower heating value
PTFE	polytetrafluoroethylene
RR	recirculation ratio
SOFC	solid oxide fuel cell

Nomenclature

Greek Symbols

δ	Turbine reaction
η	Efficiency
γ	Molar mass fraction
ω	Angular velocity in $\mathrm{rad\,s^{-1}}$
Π	Pressure ratio
ρ	Density in $\mathrm{kg\,m^{-3}}$

Roman Symbols

$\boldsymbol{F}$	Faraday constant ($96\,485.3329\,\mathrm{s\,A\,mol^{-1}}$)
$\boldsymbol{p}$	Power density in $\mathrm{W\,cm^{-2}}$
$\dot{m}$	Mass flow rate in $\mathrm{kg\,s^{-1}}$
$\dot{n}$	Molar flow rate in mol/s
A	Area in $\mathrm{cm^2}$
CD	Discharge coefficient
EAR	Excess air ratio
EWR	Excess water ratio
f_u	Fuel utilization

h Specific enthalpy in $\mathrm{J\,kg^{-1}}$

I Current in A

i Current density in $\mathrm{A\,cm^{-2}}$

LHV Lower heating value in $\mathrm{J\,mol^{-1}}$ ($LHV_{CH4} = 802\,652\,\mathrm{J\,mol^{-1}}$)

M Moment in $\mathrm{N\,m}$

n_{rot} Rotational speed in krpm

O/C Oxygen-to-carbon ratio

P Power in W

p Pressure in Pa

Re Reynolds number

RR Recirculation ratio

s Specific entropy in $\mathrm{J\,kg^{-1}\,K^{-1}}$

$S/CH4$ Steam-to-methane ratio

T Temperature in K

U Potential in V

z_e Number of electrons

z_{layer} Number of cell layers in the SOFC stack

Subscripts

amb	ambient
e	electrical
h	hydraulic
is	isentropic
mech	mechanical
rs	rotor-stator
t	total
tt	total-to-total
turb	turbine

References

[1] M. Noponen, T. Hottinen, WFC20 Biogas Unit Operation, in: Proceedings of 9th European SOFC & SOE Forum 2010, 2010 (2010).

[2] J. F. Pierre, SECA Coal-Based Systems, Tech. rep., Siemens Power Generation, Incorporated (2011). doi:10.2172/1083945.
URL https://www.osti.gov/biblio/1083945-seca-coal-based-systems

[3] M. Halinen, M. Rautanen, J. Saarinen, J. Pennanen, A. Pohjoranta, J. Kiviaho, M. Pastula, B. Nuttall, C. Rankin, B. Borglum, Performance of a 10 kW SOFC Demonstration Unit, ECS Transactions 35 (1) (2011) 113–120 (Apr. 2011). doi:10.1149/1.3569985.
URL http://ecst.ecsdl.org/content/35/1/113

[4] M. Halinen, Improving the performance of solid oxide fuel cell systems, VTT Technical Research Centre of Finland, 2015 (2015).
URL https://aaltodoc.aalto.fi:443/handle/123456789/15748

[5] G. D. Agnew, R. D. Collins, M. B. Jrger, S. H. Pyke, R. Travis, The Components of a Rolls-Royce 1 MW SOFC System, ECS Transactions 7 (1) (2007) 105–111 (May 2007). doi:10.1149/1.2729079.
URL http://ecst.ecsdl.org/content/7/1/105

[6] R. Goettler, SECA Coal-Based Systems - LGFCS, Tech. Rep. 1110772 (Aug. 2013). doi:10.2172/1110772.
URL http://www.osti.gov/servlets/purl/1110772/

[7] C. L. DeBellis, DE-FE0031180 Final Report - LGFCS Prototype System Testing - R0, Tech. Rep. DOE-LGFCS-FE0031180, 1493425 (Jan. 2019).

doi:10.2172/1493425.
URL http://www.osti.gov/servlets/purl/1493425/

[8] M. Powell, K. Meinhardt, V. Sprenkle, L. Chick, G. McVay, Demonstration of a highly efficient solid oxide fuel cell power system using adiabatic steam reforming and anode gas recirculation, Journal of Power Sources 205 (2012) 377–384 (May 2012). doi:10.1016/j.jpowsour.2012.01.098.
URL http://www.sciencedirect.com/science/article/pii/S0378775312001991

[9] H. Ghezel-Ayagh, SOFC Systems with Improved Reliability and Endurance, Tech. rep., Fuelcell Energy, Incorporated (Dec. 2016). doi:10.2172/1332289.
URL https://www.osti.gov/biblio/1332289-sofc-systems-improved-reliability-endurance

[10] R. Peters, M. Engelbracht, W. Tiedemann, I. Hoven, R. Deja, V. N. Nguyen, L. Blum, D. Stolten, Development and Test of a Solid Oxide Fuel Cell Subsystem with a Low Temperature Anode Off-Gas Recirculation, ECS Transactions 78 (1) (2017) 2489–2495 (May 2017). doi:10.1149/07801.2489ecst.
URL http://ecst.ecsdl.org/content/78/1/2489

[11] K. Weeber, P. Horstmann, J. Miersch, Changes in Power Generation and Distribution and the role of SOFC, in: Proceedings of 13th European SOFC & SOE Forum 2018, 2018 (2018).

[12] Y. Tanaka, K. Sato, A. Yamamoto, T. Kato, Development of An-

ode Off-Gas Recycle Blowers for High Efficiency SOFC Systems, ECS Transactions 57 (1) (2013) 443–450 (Jun. 2013). doi:10.1149/05701.0443ecst.
URL http://ecst.ecsdl.org/content/57/1/443

[13] J. Rechberger, M. Reissig, M. Hauth, AVL SOFC Systems on the Way of Industrialization, ECS Transactions 57 (1) (2013) 141–148 (Jun. 2013). doi:10.1149/05701.0141ecst.
URL http://ecst.ecsdl.org/content/57/1/141

[14] G. Agrawal, Advances in Fuel Cell Blowers, Tech. rep., R&D Dynamics Corporation, https://www.netl.doe.gov/sites/default/files/event-proceedings/2009/seca/presentations/Agrawal_Presentation.pdf, Accessed: 2019-10-20 (2009).

[15] H. Hooshang, High Temperature Anode Recycle Blower for Solid Oxide Fuel Cell, Website, Mohawk Innovative Technology, https://www.netl.doe.gov/research/coal/project-information/proj?k=FE0027895, Accessed: 2019-10-20 (2016).

[16] P. H. Wagner, J. Van herle, J. Schiffmann, Theoretical and Experimental Investigation of a Small-scale, High-speed, and Oil-free Radial Anode Off-gas Recirculation Fan FOR Solid Oxide Fuel Cell Systems, Journal of Engineering for Gas Turbines and Power (2019). doi:10.1115/1.4045104.

[17] P. H. Wagner, Integrated Design, Optimization, and Experimental Real-

ization of a Steam-Driven Micro Recirculation Fan for Solid Oxide Fuel Cell Systems, PhD thesis, EPFL, Lausanne, thesis number 9337 (2019).

[18] P. H. Wagner, Z. Wuillemin, S. Diethelm, J. Van herle, J. Schiffmann, Modeling and Designing of a Radial Anode Off-Gas Recirculation Fan for Solid Oxide Fuel Cell Systems, Journal of Electrochemical Energy Conversion and Storage 14 (1) (2017) 011005–011005–12 (May 2017). doi:10.1115/1.4036401.
URL http://dx.doi.org/10.1115/1.4036401

[19] M. Engelbracht, R. Peters, L. Blum, D. Stolten, Comparison of a fuel-driven and steam-driven ejector in solid oxide fuel cell systems with anode off-gas recirculation: Part-load behavior, Journal of Power Sources 277 (2015) 251–260 (Mar. 2015). doi:10.1016/j.jpowsour.2014.12.009.
URL http://www.sciencedirect.com/science/article/pii/S0378775314020266

[20] HTceramix S.A., WO 2016/087389 A1: SOFC system and method of operating a SOFC system, Patent, HTceramix S.A. (Jun. 2006).

[21] International Organization for Standardization (ISO), ISO 5167: Measurement of fluid flow by means of pressure differential devices inserted in circular cross-section conduits running full, Standard, ISO (Jun. 2003).

[22] J. Demierre, A. Rubino, J. Schiffmann, Modeling and Experimental Investigation of an Oil-Free Microcompressor-Turbine Unit for an Organic Rankine Cycle Driven Heat Pump, Journal of Engineering for Gas

Turbines and Power 137 (3) (2014) 032602–1–032602–10 (Oct. 2014). doi:10.1115/1.4028391.
URL http://dx.doi.org/10.1115/1.4028391

[23] P. Caliandro, A. Nakajo, S. Diethelm, J. Van herle, Model-assisted identification of solid oxide cell elementary processes by electrochemical impedance spectroscopy measurements, Journal of Power Sources 436 (2019) 226838 (Oct. 2019). doi:10.1016/j.jpowsour.2019.226838.
URL http://www.sciencedirect.com/science/article/pii/S0378775319308316

[24] R.-U. Dietrich, A. Lindermeir, C. Immisch, C. Spieker, C. Spitta, S. Stenger, R. Leithner, T. Kster, A. Oberland, SOFC System Using a Hot Gas Ejector for Offgas Recycling for High Efficient Power Generation from Propane, ECS Transactions 57 (1) (2013) 171–184 (Jun. 2013). doi:10.1149/05701.0171ecst.
URL http://ecst.ecsdl.org/content/57/1/171

[25] M. Hauth, J. Rechberger, S. Megel, M. Kusnezoff, Operating Results of the SOFC20 Stationary SOFC CHP System using a CFY-Stack Platform, in: Proceedings of 11th European SOFC & SOE Forum 2014, 2014 (2014).

[26] Convion, Products, Website, http://convion.fi/products/, Accessed: 2019-10-20 (2019).

[27] R. Payne, J. Love, M. Kah, Generating Electricity at 60% Electrical Efficiency from 1 - 2 kWe SOFC Products, ECS Transactions 25 (2)

(2009) 231–239 (Sep. 2009). doi:10.1149/1.3205530.
URL http://ecst.ecsdl.org/content/25/2/231

[28] Bloom Energy, Energy Server 5 datasheet, Website, https://www.bloomenergy.com/sites/default/files/es5-200kw-datasheet.pdf, Accessed: 2019-10-20 (2019).